

Strain shifts under stress-controlled oscillatory shearing in theoretical, experimental, and structural perspectives: Application to probing zero-shear viscosity

Johnny Ching-Wei Lee, Yu-Tong Hong, Katie M. Weigandt, Elizabeth G. Kelley, Hyunjoon Kong, and Simon A. Rogers

Citation: *Journal of Rheology* **63**, 863 (2019); doi: 10.1122/1.5111358

View online: <https://doi.org/10.1122/1.5111358>

View Table of Contents: <https://sor.scitation.org/toc/jor/63/6>

Published by the [The Society of Rheology](#)

ARTICLES YOU MAY BE INTERESTED IN

Rheology of crystallizing polymers: The role of spherulitic superstructures, gap height, and nucleation densities
Journal of Rheology **63**, 851 (2019); <https://doi.org/10.1122/1.5109893>

A review of thixotropy and its rheological modeling

Journal of Rheology **63**, 477 (2019); <https://doi.org/10.1122/1.5055031>

Extensional rheology of highly-entangled α -olefin molecular bottlebrushes

Journal of Rheology **63**, 917 (2019); <https://doi.org/10.1122/1.5110557>

Rheo-PIV analysis of the vane in cup flow of a viscoplastic microgel

Journal of Rheology **63**, 905 (2019); <https://doi.org/10.1122/1.5118900>

Review: Rheology of noncolloidal suspensions with non-Newtonian matrices

Journal of Rheology **63**, 705 (2019); <https://doi.org/10.1122/1.5085363>

The unification of disparate rheological measures in oscillatory shearing

Physics of Fluids **31**, 073107 (2019); <https://doi.org/10.1063/1.5106378>



The **WORLD'S** most
VERSATILE platform for
RHEOLOGICAL MEASUREMENTS

The Discovery Hybrid Rheometer





Strain shifts under stress-controlled oscillatory shearing in theoretical, experimental, and structural perspectives: Application to probing zero-shear viscosity

Johnny Ching-Wei Lee,¹ Yu-Tong Hong,¹ Katie M. Weigandt,² Elizabeth G. Kelley,² Hyunjoon Kong,¹ and Simon A. Rogers^{1,a)}

¹*Department of Chemical and Biomolecular Engineering, University of Illinois at Urbana-Champaign, Urbana, Illinois 61801*

²*Center for Neutron Research, National Institute of Standards and Technology, Gaithersburg, Maryland 20899*

(Received 24 May 2019; published 23 September 2019)

Abstract

Rheological measurements in which the applied stress or strain is oscillated are widely used to interrogate viscoelastic properties due to the independent control over the time scale and length scale afforded by changes in amplitude and frequency. Taking a nontraditional approach, we treat stress-controlled oscillatory tests as creep tests with transiently varying stress and apply an analysis typically used for steady creep and recovery experiments. Defining zero strain as the state prior to external shearing, it is shown that strain responses to small-amplitude oscillatory stressing are naturally shifted from the starting point by an amount proportional to the phase of the applied stress. The phenomenology is experimentally observed with entangled polymerlike micelles and polyethylene oxide solutions. A theory of strain shifting in the steady alternating state is provided based on recovery rheology, where differences between total strain and recoverable strains are acknowledged. User-controlled variables, such as the amplitude of the stress, the angular frequency, and the phase of the stress, as well as a lone material parameter, the zero-shear viscosity, are shown to dictate the amount of shifting. A rapid and efficient approach of determining the zero-shear viscosity is, therefore, presented. We investigate the microstructural evolution via *in situ* small-angle neutron scattering when strain shifting appears. The microscopic orientation is shown to correlate to the recoverable strain independent of the shifting. Additional measurements are carried out on collagen, pluronic-hyaluronic acid, alginate gels, and polystyrene melts to show the generic nature of the strain shift phenomenon. In addition, we demonstrate that the strain-shift knowledge can be applied to determine the horizontal shift factor in time-temperature superposition, free of any numerical fitting procedures. © 2019 The Society of Rheology. <https://doi.org/10.1122/1.5111358>

I. INTRODUCTION

To engineer soft materials with tailored flow properties requires an understanding of the molecular motion and flow behaviors of the material constituents. A material's viscoelasticity is a direct consequence of molecular motions. To this end, oscillatory shear rheology is widely used as a technique to interrogate viscoelastic properties, owing to the independent control over the time scale and length scale afforded by changes in amplitude and frequency [1–3].

Oscillatory shearing can be applied by imposing either the stress (torque) or the strain (displacement). It is standard in strain-driven oscillatory shearing to describe a material as being submitted to sinusoidal strain [4],

$$\gamma(t) = \gamma_0 \sin(\omega t), \quad (1)$$

where γ_0 and ω represent the strain amplitude and angular frequency, respectively. In this circumstance, the stress response is typically expressed as

$$\sigma(t) = \gamma_0 (G'(\omega) \sin(\omega t) + G''(\omega) \cos(\omega t)), \quad (2)$$

where the prefactors that describe how much of the stress response is in-phase and out-of-phase with the strain, $G'(\omega)$ and $G''(\omega)$, are the storage and loss moduli, respectively. Collectively, $G'(\omega)$ and $G''(\omega)$ are referred to as the dynamic moduli and have been shown to contain details of molecular motions that lead to viscoelastic responses. The dynamic moduli are proportional to the average energy stored per unit volume of the material over a cycle of the excitation and the energy dissipated per unit volume of the material over a cycle of deformation [5]. However, to accurately determine the *instantaneous* energetic terms, which would then get averaged to calculate the dynamic moduli, one must know the elastic deformation and the rate at which deformation is acquired viscously.

It is also common to refer to the stress response to oscillating strains simply in terms of the amplitude, σ_0 , and phase difference with respect to the strain, δ ,

$$\sigma(t) = \sigma_0 \sin(\omega t + \delta). \quad (3)$$

When δ is small, the stress is more in-phase with the strain, indicating a more Hookean elastic response, and when δ is close to $\frac{\pi}{2}$, the stress is in-phase with the strain rate, indicating a more Newtonian fluidlike response. If a researcher instead chooses to interrogate their material by application of stresses rather than strains, then the stresses are often said to

^{a)}Author to whom correspondence should be addressed; electronic mail: sarogers@illinois.edu

oscillate sinusoidally,

$$\sigma(t) = \sigma_0 \sin(\omega t), \quad (4)$$

where σ_0 and ω are the amplitude and the angular frequency of the applied stress. The strain response to sinusoidally varying stress is often written as

$$\gamma(t) = \sigma_0 (J'(\omega) \sin(\omega t) - J''(\omega) \cos(\omega t)), \quad (5)$$

where $J'(\omega)$ and $J''(\omega)$ are the dynamic compliances.

Despite the universal agreement regarding the formalism surrounding strain-driven oscillatory shear, in studies involving stress-controlled oscillatory shearing, researchers have used and discussed the relative merits of different phases of the applied stress. That is, in addition to the varying stress amplitudes σ_0 and frequencies ω , the applied stress can be imposed with different phases, ψ , ranging from 0 to 2π . The phase of the applied stress has not been designated an official variable according to the Society of Rheology official nomenclature [6], and so we denote it here as ψ ,

$$\sigma(t) = \sigma_0 \sin(\omega t + \psi). \quad (6)$$

The phase of the applied stress is distinct from the phase angle difference between stresses and strains, δ , used to describe the stress responses to oscillating strains. The most common example choices made regarding ψ include sine, $\sigma(t) = \sigma_0 \sin(\omega t)$, and cosine, $\sigma(t) = \sigma_0 \sin(\omega t + \pi/2)$, stresses [7–15]. Despite different researchers using different phases, there is still no consensus as to what formalism should be universally adopted. Ewoldt has suggested that cosine stresses should be adopted as standard on the basis that the signs of Fourier harmonics associated with large-amplitude sinusoidal stressing can be negative [13]. However, without clear physical understanding of what each harmonic corresponds to, or even whether individual harmonics should be viewed as having any meaning in isolation, debate about such suggestions can proceed no further than the assumed formalism allows. What is needed to resolve this discussion, and what we provide in this work, is a clear understanding of the physics of how the phase of the stress affects material responses.

The strain responses of soft materials to oscillatory stresses have been reported to oscillate about zero strain and to oscillate about nonzero values of strain. Shan and co-workers studied the nonlinear rheological behaviors of bitumen under stress-driven oscillatory shearing and reported that, under certain conditions, the strain responses oscillate about a nonzero value [14]. In their analysis, the strain responses are shifted so that they do oscillate about zero strain, and the shifting factors are presented separately. Such an analysis is reminiscent of the strain-controlled work of Munster and co-workers, who investigated fibrin and collagen networks and observed that these biopolymers change continually in the stress response to strain-driven oscillatory shearing [16]. Following a proposed shifting protocol to manipulate each cycle, they were able to construct a stress-strain master curve where responses from each cycle collapse. The phenomenon of strain shifting is not unknown and dates

back at least as far as Pipkin's lectures on the viscoelasticity theory [17]. He observed the strain shifting and specifically documented the phenomenon, "...if a fluid is subjected to a stress history $\sigma(t) = H(t) \sin(\omega t)$, then after a long time the shear (strain) oscillates sinusoidally about a nonzero value." Nonetheless, the underlying physics associated with how or why strains shift has not been systematically investigated nor have its effects on microstructure been clearly discussed.

Before discussing oscillatory stressing further, we first briefly review how responses to an imposition of a constant amount of stress for a fixed duration are described rheologically. In a creep and recovery test, as this protocol is called, it is well known that the total strain can be decomposed into recoverable (γ_{rec}) and unrecoverable (γ_{un}) components [4]. The recoverable strain is the amount of strain recovered when all stress is removed after some duration, while the unrecoverable strain is the amount of strain acquired between the start of the experiment and when all recovery has finished. In this work, we will make extensive use of the unrecoverable strain rate, $\dot{\gamma}_{\text{un}}$, which is the rate at which strain is acquired unrecoverably. The recoverable strain is associated with the steady-state compliance, while the unrecoverable strain, γ_{un} , is dictated by a combination of the applied stress, σ_0 , the duration of the stressing, t_c , and the zero-shear viscosity of the material, η_0 , $\gamma_{\text{un}} = \sigma_0 t_c / \eta_0$, as shown in Fig. 1(a) [4]. This expression arises by noting that the rate at which strain

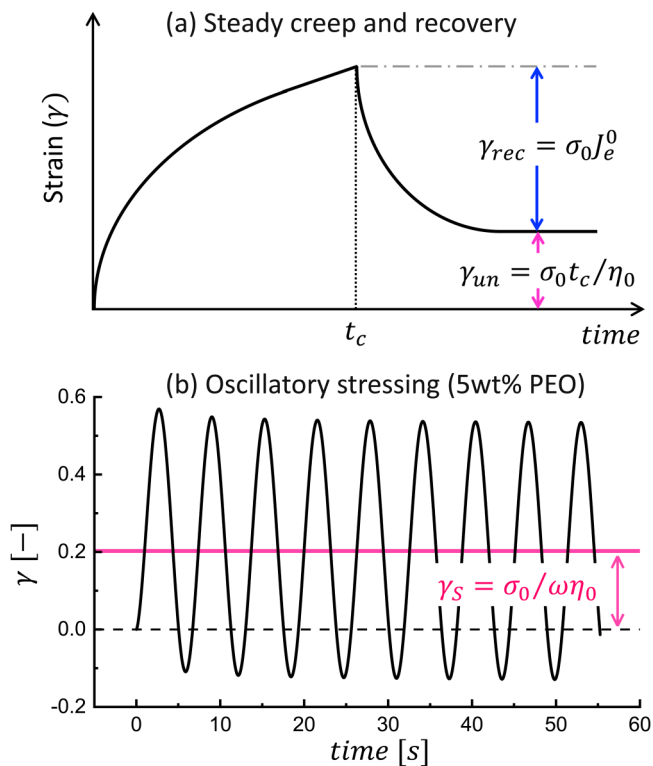


FIG. 1. (a) Strain responses from a steady creep and recovery test, where the zero-shear viscosity is known to dictate the unrecoverable strain. (Schematics adapted from Ferry's *Viscoelastic Properties of Polymers* [4].) (b) Strain responses from oscillatory sine stressing $\sigma(t) = \sigma_0 \sin(\omega t)$ from the 5 wt. % PEO solution ($\sigma_0 = 9$ Pa, $\omega = 1$ rad/s). The strain oscillates about a nonzero offset, γ_S , and the strain shift is similarly dictated by the zero-shear viscosity, $\gamma_S = \sigma_0 / \omega \eta_0$. The strain zero is defined at the state ($t = 0$ s) before applying external shear.

is acquired unrecoverably, $\dot{\gamma}_{\text{un}}$, is dictated by Newton's law of viscosity at low rates, $\dot{\gamma}_{\text{un}} = \sigma_0/\eta_0$. Integrating this expression between times $t = 0$ and $t = t_c$, which mark the onset and cessation of stress at an amplitude σ_0 , with the boundary condition $\gamma(0) = 0$, leads to the previously quoted expression for the amount of strain acquired unrecoverably. This long-accepted treatment [4] acknowledges that not all the strain is acquired recoverably. By performing recovery tests and measuring the recoverable and unrecoverable strains individually, one can, therefore, determine elastic and viscous material properties, respectively.

In this study, we view oscillatory stressing as a transient extension of the creep and recovery protocol. We follow the same line of reasoning that has been applied to the application of steady stress and derive an expression that explains why a researcher may choose to employ a particular choice of stress phase. The expression we derive shows that strain responses to oscillatory stresses can oscillate about values, γ_S , that are significantly shifted away from the point where the experiment began at zero strain. The new expression adds to the information contained in Eq. (5). We will show that this strain shift is dictated by a combination of the stress amplitude, σ_0 , the angular frequency of the oscillation, ω , and the zero-shear viscosity of the material, η_0 , in direct comparison with steady stressing, as well as *the phase of the applied stress*.

We have experimentally investigated a wide array of soft materials, and we have verified that strain responses to oscillatory stresses can indeed be displaced away from the origin as originally suggested by Pipkin [17]. Shown in Fig. 1(b) is the strain responses to sinusoidal stressing (where $\psi = 0$) from the 5 wt. % PEO solution with $\sigma_0 = 9$ Pa and $\omega = 1$ rad/s (details of this material are contained in the Experimental Section). The software that controls all commercial rheometers we are aware of will subtract this shift prior to displaying the data to the user, to ensure that they oscillate about zero strain to conform with users prior expectations. The data that are reported to researchers is, therefore, postprocessed, and the strain shifts are not reported unless the user circumvents the in-built processing, as we have done in this study.

We have recently investigated the microstructural evolution of polymerlike micelles (PLMs) and a fibrin network via *in situ* rheo-SANS and reported an out-of-equilibrium rheological structure-property relationship [15]. Specifically, we observed that the elastic modulus and shear viscosity are dictated by the *recoverable strain* and *unrecoverable strain rate*, respectively, and that the alignment of micellar segments is perfectly correlated with the recoverable strain. In addition, under small- to large-amplitude oscillatory shearing (LAOS), the microstructure, shear, and normal stresses are all correlated to the recoverable component of the strain and not the total strain. Another of our recent rheo-SANS studies showed the importance of the idea of recoverable strain as it applies to step strains under out-of-equilibrium conditions [18]. We have demonstrated that, even when a material has undergone a complex shear history, mapping the recoverable strain allows for a clear probe of the nonequilibrium relaxation modulus and other material functions. Other nonlinear

studies of colloidal and polymeric systems have also observed similar phenomena, where a constant linear-regime elasticity has been shown to exist near the strain extrema under LAOS [15,19–28]. That is, the macroscopic responses are not entirely dictated by the total strain. We also note that Wang and co-workers [29–31] have recently developed a theory of molecular elastic yielding that describes the nonlinear rheology of entangled polymers that is based on experimental studies of strain recovery. Overall, these experimental and simulation studies, as well as the microscopic yielding depiction, all suggest the importance of making a clear distinction between the recoverable and total strain, either in theoretical, structural, or rheological perspectives.

One important aspect of this work is that the zero-shear viscosity can be *efficiently* measured via the strain shift from small-amplitude oscillatory shear (SAOS) stressing without much experimental effort. The zero-shear viscosity is defined as a limiting value of viscosity at zero shear rate,

$$\eta_0 = \left. \frac{\sigma}{\dot{\gamma}} \right|_{\dot{\gamma} \rightarrow 0}. \quad (7)$$

It contains critical molecular-level information for soft materials. For instance, the scaling of the zero-shear viscosity with respect to molecular weight has been shown to be important in distinguishing entanglement in polymers. The molecular weight dependence of the zero-shear viscosity is well described by $\eta_0 \propto M^x$, where $x = 1$ and 3.4 for unentangled and entangled linear polymers, respectively [32]. The original tube model predicts the scaling of 3 for entangled linear polymers [32], while it is found that the exponent has a value of about 3.4 within a certain limit of molecular weights. A number of theoretical additions to the tube model have provided closer predictions, such as including contour length fluctuation [33] and constraint release [34]. The scaling of the zero-shear viscosity has also been shown to reveal topological differences. Dalsin *et al.* [35] observed that, for their bottlebrush polymers, a weak dependence ($\eta_0 \propto M^a$, $a < 0.5$) exists at low molecular weight, and the scaling transitions into Rouse-like dynamics ($a = 1.2$) at high molecular weight. In equilibrium dynamics, such as that measured in SAOS, the zero-shear viscosity is a manifestation of diffusion processes of microscopic entities. The zero-shear viscosity, therefore, is an important material property in developing either simple models like the linear or corotational Maxwell models [36] or other physical models that include hydrodynamic interactions, reptation dynamics, or convective constraint release (CCR) processes [32].

In bulk rheometry, the zero-shear viscosity is typically measured by imposing steady, unidirectional shear deformation on a material. The resulting steady-state shear stress is recorded, and the zero-shear viscosity is either directly determined as the ratio of the shear stress to the shear rate or indirectly determined by extrapolating from an *accessible* portion of the flow curve. While the determination is accessible for most polymer solutions, problems arise in polymer melts. Inevitably, the accuracy of determination depends on a number of experimental variables including the geometry that is used for the measurements. To reach steady state,

measurement times can be excessively long, depending on molecular weights and temperatures. A stable flowing state may not even be experimentally accessible. For example, gravity can induce distortions in the shape of the material in the filled gap, and chemical degradation can occur over the course of a measurement, especially if an inert atmosphere is not supplied. Further, steady-shear protocols involve constantly deforming melts in one fixed direction and often result in edge fracture, which critically changes the accuracy of measurements [37].

A few alternatives have been suggested to avoid such artifacts. The cone-partitioned-plate (CPP) geometry has been designed [38,39] to postpone or reduce the influence of edge fracture on measurements. Strain-controlled SAOS is another protocol that has been widely used to interrogate materials while limiting deformations that could lead to flow instabilities. While the conventional SAOS protocol does not directly measure the steady-shear viscosity (or the zero-shear viscosity), the terminal-regime data are typically taken to indirectly inform the zero-shear viscosity as $\eta_0 = \lim_{\omega \rightarrow 0} G''/\omega$. The well-known phenomenological Cox–Merz rule [40] has also been demonstrated to successfully correlate the complex viscosity from SAOS with the steady-shear viscosity, $\eta^*(\omega) = \eta(\dot{\gamma})|_{\omega=\dot{\gamma}}$, for mostly linear homopolymers.

The importance of the zero-shear viscosity has clearly been established. We demonstrate in this work a rapid and reliable method for determining the zero-shear viscosity based on the strain shifts observed in oscillatory stressing. We first briefly introduce the concepts of recovery rheology and present an associated theoretical framework that predicts strain shifts. The phenomenology and theory are subsequently demonstrated with experimental data from PLMs and an entangled polyethylene oxide (PEO) solution. Exploiting *in situ* time-resolved rheo-SANS, we further show that the structural evolution of the micellar solution is entirely dictated by the recoverable portion of strain, despite the significantly different amounts of total strain that are measured. The technique is further applied to numerous stiff biopolymer gels including thermoreversible pluronic-hyaluronic acid (PI-HA), alginate, and collagen. We show that the strain responses of the soft viscoelastic precursor solutions clearly shift from the origin, whereas their corresponding (stiffer) predominantly elastic gels exhibit strains with little-to-no shifts, confirming the theory that the shift originates from the viscous flow properties. Finally, we demonstrate that the understanding and phenomenology can be extended to entangled polymer melts, providing an accessible way to measure the zero-shear viscosity of melts, and in turn, experimentally determine the shift factors required for time-temperature-superposition (TTS) [4].

II. EXPERIMENTAL SECTION

A. Materials

1. Polymerlike micelles

The PLMs studied in this work are an aqueous solution of cetylpyridinium chloride (CPCI) and sodium salicylate (NaSal) in 0.5M NaCl and D₂O brine (Sigma-Aldrich). D₂O is used to increase scattering contrast. The solution of

8 wt. % CPCI in brine with molar ratio of NaSal (Sigma-Aldrich) to CPCI (Spectrum Laboratory) of 0.5 was prepared at least 2 days before experiments. The rheological experiments from the micellar solution were conducted at 25 °C.

2. Polyethylene oxide solution

The PEO solution is prepared in dimethyl sulfoxide (DMSO), where the PEO (Sigma-Aldrich) has a molecular weight of 1 000 000 g/mol, and DMSO (Fisher scientific) is chosen as the solvent for its good solubility and low evaporation (boiling point ≈ 189 °C). The solution was gently stirred at 60 °C on a hot plate for 24 h and incubated in a water bath at 45 °C for 24 h before experiments were conducted at 45 °C.

3. Polystyrene

Narrowly dispersed polystyrene (PS) samples were synthesized via an anionic polymerization of styrene using a secBuLi initiator [41]. PS samples ($T_g \approx 100$ °C) were made and characterized by gel permeation chromatography (GPC) with $M_n = 45\,900$ g/mol, $M_w/M_n = 1.02$ (PS-46k) and $M_n = 14\,400$ g/mol, $M_w/M_n = 1.01$ (PS-14k).

4. Collagen

The sol-state of collagen consists of type I bovine collagen solution (3 mg/ml in 0.01N hydrochloric acid; PureCol, Advanced BioMatrix). Collagen gels were prepared by gently mixing 1.2 ml type I bovine collagen solution with 125 μ l of the reconstituting solution (0.26M sodium bicarbonate, 0.2M HEPES, and 0.04 N NaOH). The pregel solution was immediately transferred to the bottom plate of the rheometer, and the measurements were taken after 3 h. The temperature is maintained at 25 °C throughout with low-viscosity mineral oil to prevent dehydration.

5. Pluronic-hyaluronic acid

Pluronic (Pluronic F-127; Sigma-Aldrich)-hyaluronic acid solution (Sodium Hyaluronate Pharma Grade 150; Novamatrix) was prepared by dissolving 2 g of pluronic and 50 mg of hyaluronic acid in 10 ml of water. The solution was mixed overnight in a vial maintained at 4 °C. The PI-HA solution is thermoresponsive. The sol-state is measured at a temperature of 15 °C, while the gel-state is achieved by maintaining temperature at 30 °C for 1 h before measurements.

6. Alginate

Alginate (100 mg, 0.5 mmol uronic acid, FMC Biopolymer Inc.) was dissolved overnight in 0.1M 2-morpholinoethanesulfonic acid buffer (pH 6) at a concentration of 3 wt. %, which is measured as the sol-state. Hydroxybenzotriazole (0.25 mmol) and adipic acid dihydrazide (0.1 mmol) were added sequentially under continuous stirring. 1-Ethyl-3-(3-dimethylaminopropyl)carbodiimide (0.25 mmol) was then added, mixed, and transferred promptly to the bottom plate of the rheometer. The temperature is maintained at 25 °C throughout with low-viscosity mineral oil to prevent dehydration.

B. Rheometry

Rheological measurements are performed on a DHR-3 stress-controlled rheometer (TA Instruments), where the temperature is controlled via a Peltier system at the desired temperature for each material. All the polymeric solutions are tested with a 4-degree cone and plate fixture with 40 mm diameter. The measurements of PS melts are carried out in an inert environment via an environmental test chamber to prevent degradation and 8 mm parallel plates are used for melt rheometry with an approximately 1 mm gap.

Stress-controlled oscillatory shearing is commanded within the arbitrary wave test environment in TRIOS (TA Instruments) where the recorded raw response is accessed without data processing that eliminates shift information in predefined oscillatory testing procedures. Strain responses during the steady-alternating state are used to determine the strain shifts, γ_S . All the results are replicated at least three times to confirm reproducibility.

Recoverable and unrecoverable strains are measured by performing constrained recovery tests [42,43] in the steady-alternating state when all initial transience has decayed. An iterative constrained recovery procedure [15] is employed in which the shear stress is abruptly set to zero ($\sigma = 0$), and the constrained recovery is recorded for a series of discrete instances along a cycle of oscillation. The unrecoverable strain, γ_{un} , is defined as the strain where the system ultimately recovers to, and the recoverable strain, γ_{rec} , is the difference between the strain at the moment the stress is removed and the unrecoverable strain,

$$\gamma_{rec}(t) = \gamma(t) - \gamma_{un}(t). \quad (8)$$

All the constrained recovery tests are performed until equilibrium is achieved.

The linear viscoelasticity of PS is measured by performing dynamic frequency sweeps over the temperature range of 110 to 180 °C in a stable Nitrogen environment with 8 mm parallel plates. A master curve is constructed by TTS principles [4]. The temperature-dependence of the corresponding horizontal shifting factors a_T is well-described by the Williams–Landel–Ferry (WLF) model

$$\log(a_T) = \frac{-C_1(T - T_{ref})}{C_2 + T - T_{ref}}, \quad (9)$$

where T and T_{ref} represent measurement and reference temperatures.

C. Rheo-small-angle neutron scattering

Rheo-small-angle neutron scattering (Rheo-SANS) experiments are conducted at the NIST Center for Neutron Research on the SANS beamline NGB-30; a stress-controlled MCR501 rheometer (Anton Paar) with a concentric cylinder Couette geometry operating in its native stress-controlled mode is used for all experiments. The rheo-SANS is configured to have a neutron wavelength of 6 Å and the detector is located 8.235 m from the sample, while the reference static SANS is configured to have a neutron wavelength of 6 Å and

three detector distances of 1, 4, and 13 m. The two configurations cover a momentum transfer vector (q -vector) ranging from 0.006 to 0.03 1/Å (rheo-SANS) and 0.004 to 0.2 1/Å (static SANS), respectively. Temperature is maintained at 25 °C for all the SANS experiments.

Time-resolved SANS methods [44] are used to continuously monitor the microstructural change of PLMs under oscillatory shearing and the 2D SANS data are reduced following the NCNR guidelines [45], with a temporal deconvolution protocol [46] to enhance the resolution and accuracy of the underlying structural evolution.

III. RESULTS AND DISCUSSION

A. Constrained recovery tests

Strain can be decomposed into recoverable and unrecoverable components by performing (constrained) recovery tests. The idea was first proposed by Weissenberg [42] and Lodge [43]. Lodge noted that a typical recovery test is geometrically constrained in one dimension and, therefore, referred to this protocol as a *constrained* recovery test.

The recovery concept has been applied to study numerous soft polymeric materials [43,47–53]. We have recently explored the implications of recoverable and unrecoverable strain on oscillatory shearing, where we demonstrated that rich structural and rheological information can be obtained by coupling oscillatory shearing with constrained recovery [15].

In this study, we perform a series of constrained recovery tests following small-amplitude sinusoidal stressing ($\sigma(t) = \sigma_0 \sin(\omega t)$) on the two polymeric solutions. Exemplary data are shown in Fig. 2 from the PLMs and the PEO solutions at 0.5 and 1.4 rad/s, respectively. The collapse of the strain response in the first interval confirms that the materials have reached their steady-alternating states and experience the same oscillatory shear history before the constrained recovery tests are performed. The recovery tests (color curves) define the second interval and show that the amount of recoverable and unrecoverable strain varies during a period of oscillation. These features are reported and discussed in more depth in our recent work [15].

Two additional phenomena can be observed in both the cases in Fig. 2. In the first interval, where oscillatory stress is applied, the total strain (gray curves) is shifted away from the origin, where the experiments began. We denote the finite strain about which the responses oscillate γ_S . Additionally, we observe that the unrecoverable strain oscillates about the same shifted strain γ_S . Averaging the time-varying unrecoverable strain $\gamma_{un}(t)$ over an oscillation also defines γ_S .

B. A theoretical description of strain shifts

In this section, we follow the same line of reasoning as applied to creep and recovery tests in which constant amounts of stress are applied for finite intervals. We extend those arguments to allow for time-varying stresses, particularly sinusoidally oscillating stresses with a prescribed phase. We develop here a theoretical description of strain shifts observed in oscillatory stress-controlled rheometry. We start by noting that strain can be decomposed into a sum of

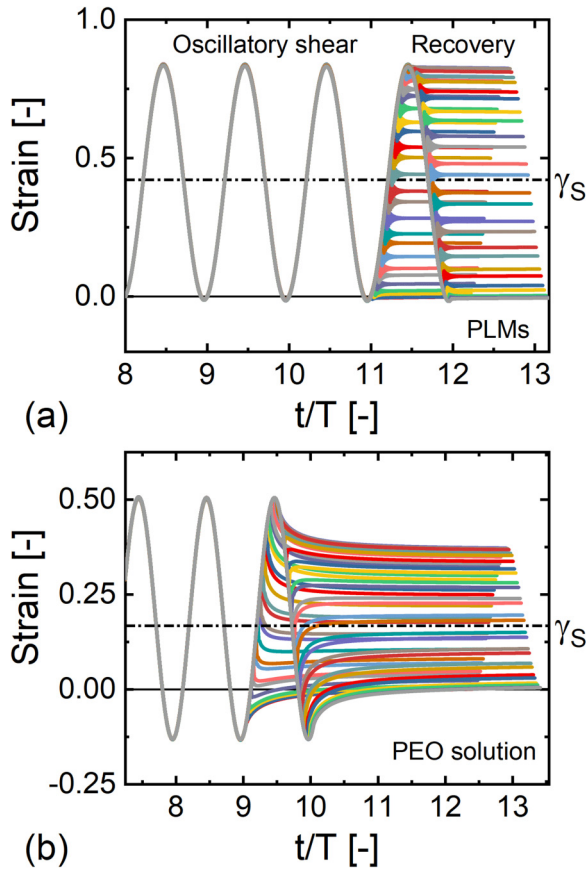


FIG. 2. Oscillatory stressing followed by constrained recovery tests from (a) PLMs, $\gamma_s = 0.424$ and (b) PEO solution, $\gamma_s = 0.169$.

recoverable and unrecoverable components. The recoverable strain is deformation that is elastic, while the viscous properties are dictated by the rate at which the strain is acquired unrecoverably. Steady flowing properties, such as the shear viscosity η , are therefore accurately described as the ratio of shear stress and the unrecoverable strain rate [15],

$$\eta = \sigma / \dot{\gamma}_{un}. \quad (10)$$

This relationship has been demonstrated in our recent study of LAOS, in which we show that by measuring the unrecoverable strain rate $\dot{\gamma}_{un}$, the shear viscosity η under oscillatory shearing can be defined following Eq. (10) and is consistent with the viscosity probed from steady-shearing tests. We note that, for a simple Newtonian liquid, all the strain is acquired unrecoverably, and the (total) shear rate, therefore, equivalently corresponds to the unrecoverable strain rate. However, the same is not true for a viscoelastic system, and it is imperative to experimentally decompose the total strain.

We begin by examining this relationship under SAOS with the PLMs and PEO solutions. A series of constrained recovery tests are performed iteratively in the alternance state on both polymeric solutions, where the imposed amplitudes are purposely limited to the linear regime. The stress is plotted as a function of unrecoverable strain rate in Fig. 3 for both solutions across a range of frequencies. Straight lines with a constant slope are obtained from tests performed at Deborah numbers ($De = \lambda\omega$, where λ is the longest

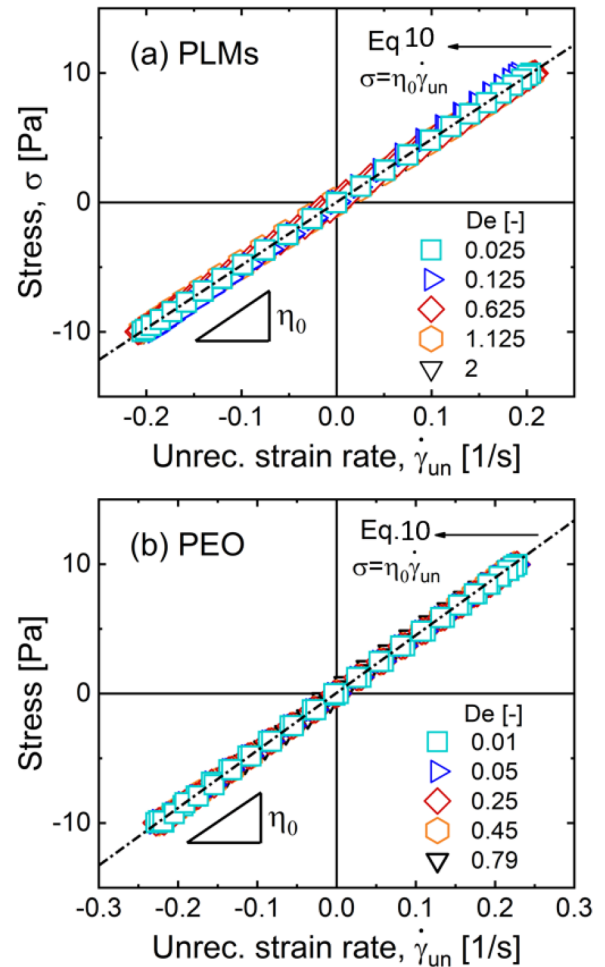


FIG. 3. Viscous Lissajous curve of stress versus unrecoverable strain rate $\sigma - \dot{\gamma}_{un}$ from (a) PLMs and (b) PEO solutions. The dashed line is the prediction from Eq. (11).

relaxation time and ω is the imposed frequency) up to 2, where inertia issues associated with the stress-controlled protocol are negligible. Reference lines that have slopes equal to the zero-shear viscosities η_0 determined from steady-shear tests are presented in Fig. 3 as dashed lines. The data collected across various De show excellent agreement with the reference lines [Eq. (11)]. This indicates that, when the unrecoverable strain rate is small, the viscosity in Eq. (10) is the zero-shear viscosity.

Having experimentally confirmed Eq. (10) under oscillatory stressing, we now extend this understanding and present a theoretical argument of strain shifts. We define the total and unrecoverable strains prior to any shear deformation to be zero, $\gamma(0) = 0$, $\gamma_{un}(0) = 0$, and we generically refer to linear-regime oscillatory stressing as having the form $\sigma(t) = \sigma_0 \sin(\omega t + \psi)$. In this representation, which we view as an oscillatory creep/recovery protocol, the unrecoverable strain rate can be expressed via Newton's law of viscosity, as

$$\dot{\gamma}_{un}(t) = \frac{\sigma(t)}{\eta_0} = \frac{\sigma_0 \sin(\omega t + \psi)}{\eta_0}. \quad (11)$$

An expression for the amount of unrecoverable strain can, therefore, be derived by integrating Eq. (11) from the state

prior to any shearing ($\hat{t} = 0$) to the current time ($\hat{t} = t$),

$$\gamma_{\text{un}}(t) = \int_0^t \dot{\gamma}_{\text{un}}(\hat{t}) d\hat{t} = \int_0^t \frac{\sigma_0 \sin(\omega \hat{t} + \psi)}{\eta_0} d\hat{t}, \quad (12)$$

where \hat{t} is a dummy variable of time. An expression for the unrecoverable strain at an arbitrary time is, therefore,

$$\gamma_{\text{un}}(t) = \frac{\sigma_0}{\omega \eta_0} \cos \psi - \frac{\sigma_0}{\omega \eta_0} \cos(\omega t + \psi). \quad (13)$$

That is, the unrecoverable strain is made up of two terms. One of the terms varies cosinusoidally in time, and the other is a constant offset that depends on the phase of the applied stress.

The strain shift we have just derived comes from a purely viscous contribution, as elasticity leads to only recoverable deformation. One can easily relate the recoverable strain to the shear stress,

$$\gamma_{\text{rec}}(t) = \frac{\sigma(t)}{G_{\text{rec}}} = \frac{\sigma_0 \sin(\omega t + \psi)}{G_{\text{rec}}}, \quad (14)$$

where G_{rec} is an elastic (recoverable) modulus in a force-extension perspective, resulting in a sinusoidal form that oscillates about zero strain. We denote the elastic (recoverable) modulus, which is determined from the recoverable strain and is the inverse of the recoverable compliance defined in the official nomenclature [6] of the Society of Rheology $1/J_r^s$, as G_{rec} to distinguish from the traditional relaxation modulus. Combining Eqs. (13) and (14), we confirm that the strain shift only comes from the viscous contribution in Eq. (13). Indeed, the results in Fig. 2 indicate that the total strain and the (viscous) unrecoverable strain share the same offset. The strain shift, γ_S , from small-amplitude oscillatory shear stressing is, therefore, established as

$$\gamma_S = \frac{\sigma_0}{\omega \eta_0} \cos \psi. \quad (15)$$

The theoretical expression in Eq. (15) has the same form as that of the unrecoverable strain in a steady creep and recovery test [Fig. 1(b)]. They are both of the form (stress \times time/viscosity). That is, they both contain information about the zero-shear viscosity and experimentally controlled parameters. The major difference between the two expressions is that the new expression that describes oscillatory shearing contains information regarding the *phase* of the applied stress. It is, therefore, possible to change the position about which strain responses oscillate just by changing the phase of the imposed stress. To get maximum shifting away from zero strain, phases of $\psi = 0$ or $\psi = \pi$ should be used, while any oscillatory strain response can be made to oscillate about zero strain by choosing $\psi = \pi/2$ or $\psi = 3\pi/2$. A full description of the strain response to steady-alternating small-amplitude oscillatory stressing ($\sigma(t) = \sigma_0 \sin(\omega t + \psi)$), originally presented as Eq. (5) becomes

$$\gamma(t) = \sigma_0 \left(J'(\omega) \sin(\omega t + \psi) - J''(\omega) \cos(\omega t + \psi) + \frac{\cos \psi}{\omega \eta_0} \right). \quad (16)$$

We note that this offset term in strain responses typically appears as a generic term in the literature, if it is included at all. For instance, see Eq. (12) in Ewoldt's work [13], where the offset is denoted as " $\gamma(\omega, \sigma_0)$." Here, for the first time, the exact expression of this offset term is provided in small-amplitude oscillatory stressing. As with any constant offset, it does not affect the information content such as the dynamic compliances of the oscillating portion of the response. While the Cox–Merz approach of determining the zero-shear viscosity from the dynamic compliances, or the dynamic moduli, involves a sweep of the lowest frequencies accessible, our new expression makes it clear that the zero-shear viscosity can also be obtained from a single test, in principle at any frequency, by observing the strain shift.

Equation (15) involves a number of user-defined parameters, including the stress amplitude σ_0 , the angular frequency ω , and the phase of the imposed stress ψ , as well as one material function, the zero-shear viscosity η_0 . As long as a material is perturbed in the linear regime, one can efficiently determine the zero-shear viscosity through the observed strain shift. In the subsequent sections, we perform a series of experiments to verify this theoretical prediction and demonstrate the generality and applicability of this approach with a wide array of materials.

C. Experimental strain shifts

To experimentally study the effects of the frequency and the phase of the imposed stress on strain shift, a series of stress-controlled oscillatory shear tests is performed in the linear regime. With imposed frequencies ranging from 0.1 to 4.5 rad/s ($De = 0.025$ – 1.1 for PLMs and $De = 0.01$ – 0.45 for PEO), the resulted strain shift γ_S under the steady-alternating state is extracted and presented in Fig. 4. Both the investigated polymeric solutions show that the strain shift scales with the inverse of the frequency, $\gamma_S \propto \omega^{-1}$, in agreement with the theoretical description in Eq. (15).

The dependence on the phase of the imposed stress ψ is studied by varying ψ from 0 to 2π at various frequencies. The strain shift is plotted as a function of ψ in Fig. 5. With the stress phase changing in between 0 and 2π , the strain shift clearly evolves in a cosinusoidal form, and the magnitude of the strain shift increases with the decreasing frequency. We observe maximum positive and negative strain shifts at stress phases ψ of 0 and π , respectively, and no strain shift when the stress phase is $\pi/2$ or $3\pi/2$. These experimental observations agree with the theoretical description provided by Eq. (15), which predicts that the strain shift is linearly proportional to the cosine of the stress phase, $S_\gamma \propto \cos(\psi)$.

The experimental strain shifts determined under a variety of flow conditions can be superimposed to form a master curve. In Fig. 6, we plot the strain shifts as a function of $\sigma_0 \cos \psi / \omega$ from both the PLM and PEO solutions. Regardless of the frequencies and stress phases imposed, the strain shifts collapse to form a single master curve described by Eq. (15) (indicated as dashed lines in Fig. 6). The slopes of these lines are equal to the inverse of the zero-shear viscosity.

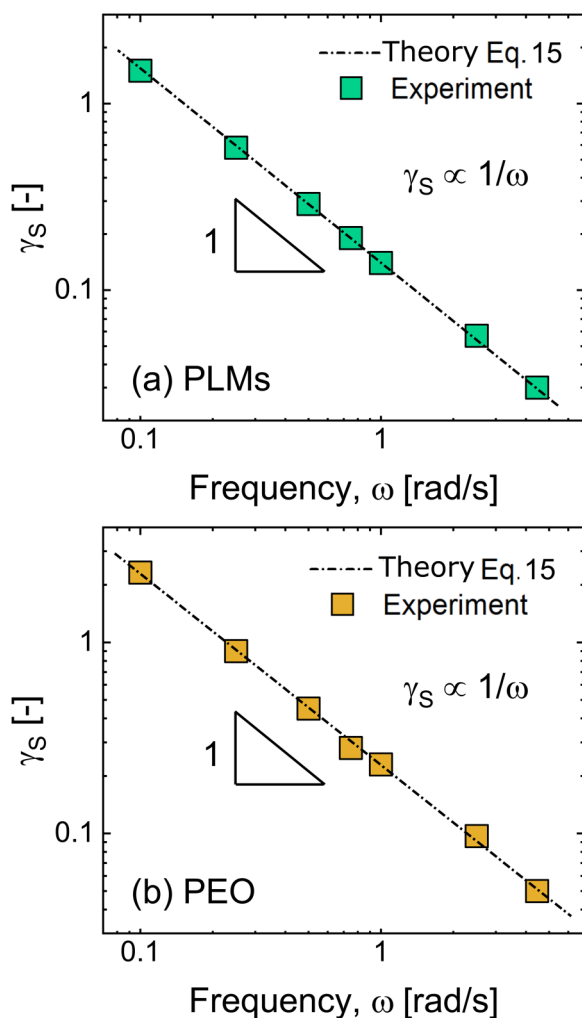


FIG. 4. The strain shifts γ_S from oscillatory stressing $\sigma = \sigma_0 \sin(\omega t)$ are plotted as the function of applied frequency ω from (a) PLMs and (b) PEO solutions, where the frequency dependence of $\gamma_S \propto \omega^{-1}$ predicted from Eq. (15) is observed. The stress amplitudes are 6.8 Pa (PLMs) and 10 Pa (PEO), both in the linear regime for the materials.

D. On probing zero-shear viscosity

We have demonstrated that an experimental master curve can be constructed on the basis of a simple set of arguments that make a clear distinction between recoverable and unrecoverable strains (Fig. 6). This informative master curve directly and efficiently gives researchers access to the zero-shear viscosity, η_0 .

In Fig. 6, the zero-shear viscosities of both the PLMs and PEO solutions can be accurately obtained from the strain shifts. The zero-shear viscosity corresponds to the inverse of the slope of the master curves and matches the results obtained from steady shearing. For the purpose of demonstration, the data in Fig. 6 are taken from an extensive array of experimental conditions; in practice, however, the determination of the zero-shear viscosity need not be as intensive. Determination can be efficiently achieved by measuring the strain shift from only one carefully chosen condition. Given that the SAOS protocol is already an established part of any rheological characterization of soft materials, this piece of information is, therefore, readily available and requires little

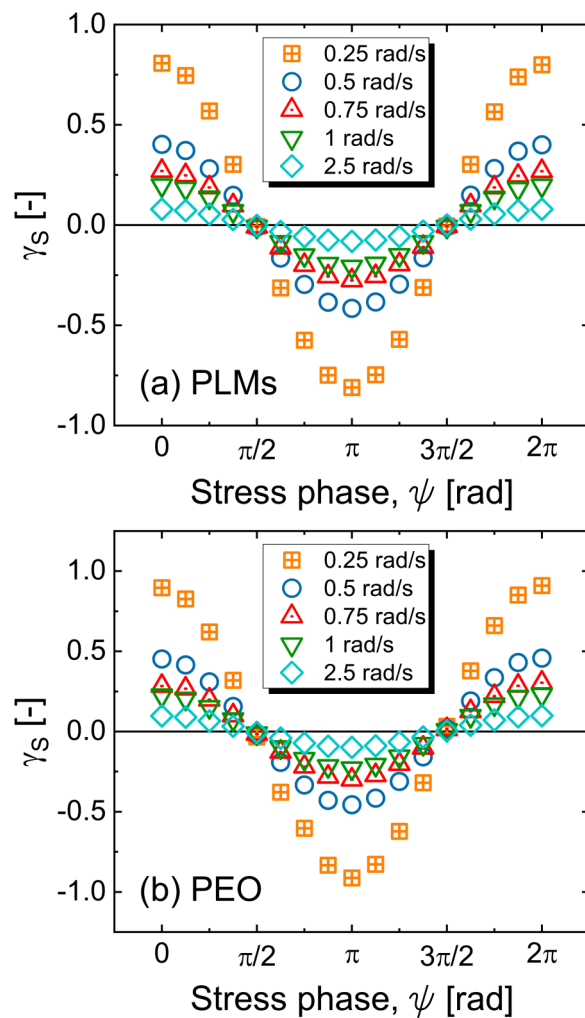


FIG. 5. The strain shift γ_S from oscillatory stress input of $\sigma = \sigma_0 \sin(\omega t + \psi)$ is plotted as a function of stress phases ψ at the frequency of 0.25, 0.5, 0.75, 1, and 2.5 rad/s from (a) PLMs and (b) PEO solutions.

extra experimental effort to obtain. This rapid determination is particularly important and useful for materials that undergo chemical changes in a short period of time, and for those that fracture at their edges in steady-shear deformation, such as biological gels and polymer melts. We discuss these specific cases in Sec. III F.

E. Microstructure with shifted strain

The phenomenon of strain shifts has been both theoretically and experimentally established. In this section, we show that the structure, as determined by SANS, is unaffected by the shifted strains. Instead, we observe that the structure is directly correlated to the recoverable component of the total strain. We use time-resolved rheo-SANS and simultaneously monitor the structure change of PLMs under oscillatory shearing when the strain shifts.

An asymmetric (total) strain suggests that a material is being strained more in one direction than in the other. Such strain responses, therefore, imply that the time-resolved microscopic structure ought also to be asymmetric. This argument, however, is solely based on the viewpoint of the total (lab-frame) strain, where the reference state is always

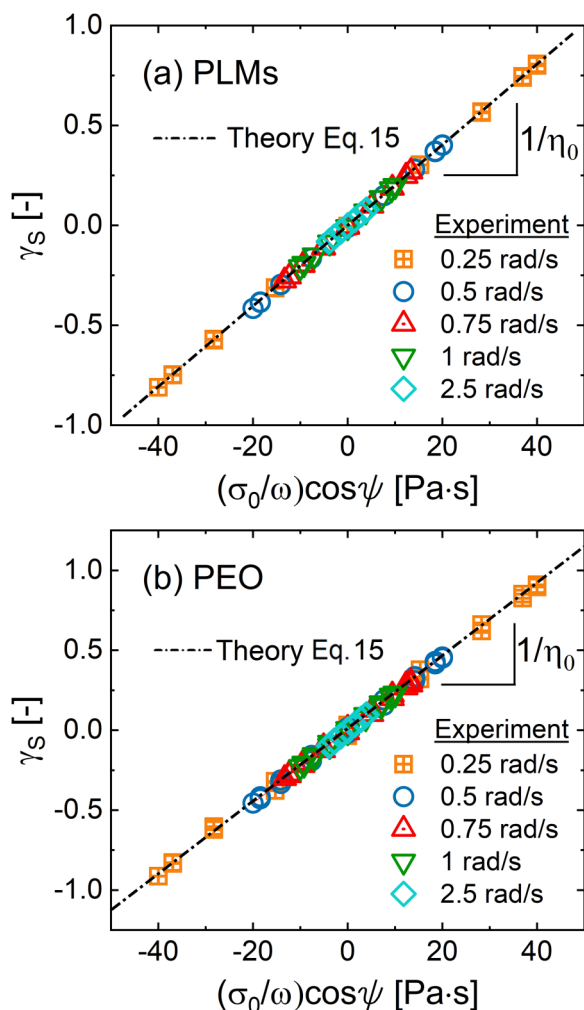


FIG. 6. A master curve of strain shifts for PLMs (a) and PEO (b) solutions. The strain shifts γ_s from distinct flow conditions (i.e., varying frequencies ω and stress phases ψ) can be superimposed to construct a master curve by plotting against $(\sigma_0/\omega)\cos\psi$ according to Eq. (15). The slope of the master curve, $1/\eta_0$, provides an accurate approach to probe the zero-shear viscosity, which is determined to be 48 Pa s (PLMs) and 45 Pa s (PEO).

considered as the origin. Following the definition of Weissenberg [42] and Reiner [54], the *material-frame* strain is the *recoverable strain*, where the reference state (or “ground state” as originally stated by Weissenberg) is considered to be the strain to where the materials recover when shear stresses are released. To phrase this another way, Weissenberg considered the unrecoverable strain as the reference state. To investigate the difference and correlation between these two distinct viewpoints and structure, we examine the underlying PLMs microstructure and compare it with the lab-frame (total) and material-frame (recoverable) strains.

An isotropic 2D SANS pattern indicates that the structure has no particular orientation and retains its equilibrium configuration. In such cases, the 2D scattering patterns can be reduced in complexity further, by integrating azimuthally, to obtain a 1D scattering intensity as a function of scattering vector, creating an I - q curve. However, once a flow field is applied to a polymeric sample, the chains begin to align in the flow direction. The flow-induced alignment can be

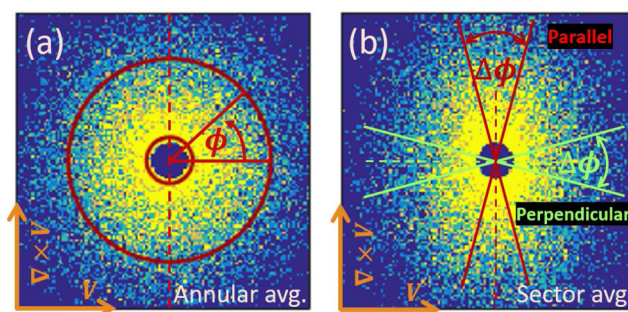


FIG. 7. A schematic of SANS reducing methods. (a) Annular averaging, the intensity $I(\phi)$ is calculated over the defined annulus ($q^* = 0.006\text{--}0.03\text{ 1/\AA}$) over azimuthal angle ϕ of $0^\circ\text{--}360^\circ$. (b) Sector averaging, the intensity $I(q, \phi)$ is calculated on two sectors parallel ($\phi = 90^\circ \pm 10^\circ$) and perpendicular ($\phi = 0^\circ \pm 10^\circ$) to the orientation angle ($\phi_0 = 90^\circ$), respectively.

revealed from the 2D scattering patterns. As an example, the structures with their equilibrium configuration and flow-induced alignment are demonstrated in Figs. 7(a) and 7(b), respectively. The corresponding isotropic and anisotropic 2D scattering patterns contain information regarding how the structure responds to the flow.

To quantify the degree of anisotropy and scattering intensity on different length scales, 2D scattering patterns are typically reduced to simpler vectors or scalars. Rheo-SANS often involves shear-induced orientation in 2D SANS data and requires methods that consider scattering at each angle and length scale separately. Such methods include the annular average method [Fig. 7(a)], which calculates the intensity at each azimuthal angle ϕ over a fixed range of q -vector, referred to as q^* . The q^* used in this study focuses on the segmental length of micelles [15], $q^* = 0.006\text{--}0.03\text{ 1/\AA}$. To focus on particular orientations, a sector average method is additionally used [Fig. 7(b)], where the scattering from particular sectors is integrated to produce an I - q curve for that sector. In the following analysis, we choose two sectors, one *parallel* ($\phi = 90^\circ \pm 10^\circ$) and one *perpendicular* ($\phi = 0^\circ \pm 10^\circ$) to the flow direction ($\phi_0 = 90^\circ$). We note that scattered signal represents the Fourier transform of the real-space orientation. The transformation imparts a 90° rotation so that the sectors labeled parallel and perpendicular are, therefore, aligned with and orthogonal to the flow direction, respectively.

The static 1D SANS from PLMs at rest is displayed in Fig. 8 as black squares. This quiescent scattering is characteristic of micellar structure. Microscopically, the segments of the micellar structure behave as cylindrical rods and exhibit rodlike scattering where $I \propto q^{-1}$. The segmental length scale (q^*) is highlighted in Fig. 8(a) as shaded blue, where rodlike scattering features are observed. Stress-controlled oscillatory rheo-SANS measurements are performed with varying imposed stress phases ψ ranging from 0 to $7\pi/4$, where the strain shift changes significantly. The resulting 1D SANS is time-averaged over a cycle of oscillation and presented in Fig. 8(a). Evidently, the micellar scattering characteristics are retained under oscillatory shearing, suggesting the micellar phase persists in all the testing conditions.

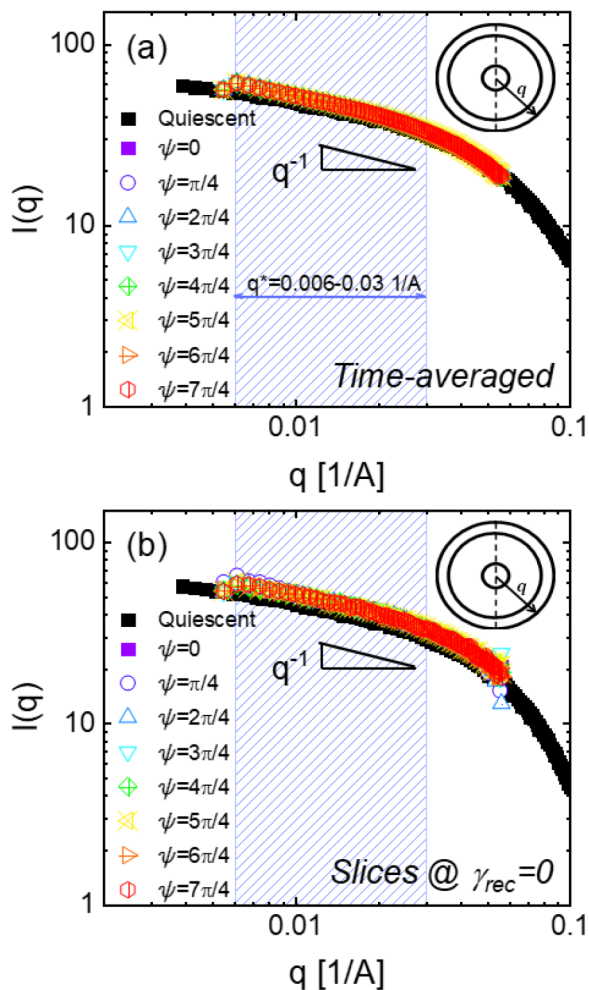


FIG. 8. 1D circular-average scattering intensity $I(q)$ over a cycle of oscillation (time-averaged) (a), at the instants when $\gamma_{\text{rec}} = 0$ (b). Rheo-SANS is performed with different imposed stress phases $\psi = 0, \pi/4, 2\pi/4, 3\pi/4, 4\pi/4, 5\pi/4, 6\pi/4,$ and $7\pi/4$, in comparison with the quiescent scattering (black). The blue shaded regime represents the q^* range where the segmental rodlike scattering $I \propto q^{-1}$ is observed.

We show in Fig. 8(b) the azimuthally averaged I - q curve from the instants when the recoverable strain is zero under oscillatory shearing. At the moments of $\gamma_{\text{rec}} = 0$, the 2D scattering patterns are isotropic, regardless of the phase of the imposed stress ψ as shown in Fig. 10. We, therefore, adopt the circular-average method to compare with the quiescent equilibrium scattering. As shown in Fig. 8(b), the identical I - q features indicate that the equilibrium structure is observed at the instants when the recoverable strain is zero. This observation is consistent with our recent findings [15].

To further study the correlation between the structure and the recoverable strain, we examine the structure at the moments when the recoverable strain is zero and when it is largest. We perform these tests with different stress phase angles $\psi = 0, \pi/4, 2\pi/4$, using annular-averaged and sector-averaged methods (see supplementary material [73] for all other ψ). In the case of zero recoverable strain, the intensity is independent of azimuthal angle [Fig. 9(a)], indicating isotropic scattering. Further, both the parallel and perpendicular sectors are indistinguishable from the quiescent scattering [Fig. 9(b)]. These results confirm that the equilibrium

structure is restored when the recoverable strain is zero. In contrast, at the instant of maximum recoverable strain, the scattering is clearly anisotropic, as the intensity has two significant peaks at angles of $\phi = 90^\circ$ and 270° [Fig. 9(c)]. The micellar segments are, therefore, more aligned when the recoverable strain is largest. When the recoverable strain is largest, the sector-averaged method [Fig. 9(d)] shows that the two sectors differ in their intensities. A slightly decreased intensity in the perpendicular direction and an increase in the parallel sector reveals that a significant fraction of segments are being aligned in the flow direction.

To quantify the temporal alignment of the micellar Kuhn segments [44], we define an alignment factor A_f as

$$A_f = \frac{\int_0^{2\pi} I_c(q^*, \phi) \cos(2(\phi - \phi_0)) d\phi}{\int_0^{2\pi} I_c(q^*) d\phi}, \quad (17)$$

where $I_c(q^*, \phi)$ is the azimuthal intensity over q^* and ϕ is the azimuthal angle. ϕ_0 represents the orientation angle, which in this geometry is the flow direction.

The temporal alignment factor is presented as a function of normalized time in Fig. 10 for a variety of imposed stress phases ($\psi = 0, \pi/4, 2\pi/4, 3\pi/4$) at 1 rad/s. We first focus on the evolution of the alignment factor and total strain in the left panel. While the (total) strain shifts from the origin (γ_s indicated by dashed line) with varying imposed stress phases ψ as predicted by Eq. (15), the microscopic SANS data show that the structure evolves symmetrically over the course of the oscillation. That is, while the total strain and the alignment factor exhibit changing phase differences, the total strain extrema [for instance, about 8 and 0 in Fig. 10(a)] give rise to the same amount of structural alignment. This result suggests that the total strain is not meaningfully correlated with the structural alignment.

Following the proposal of Weissenberg [42] by performing an extensive series of constrained recovery tests, we present the recoverable (material-frame) strain in the right panel in Fig. 10. The recoverable strain evolves distinctly from the total strain. For instance, at $t/T \approx 0.5$ with a stress phase of $\psi = 0$, the recoverable strain is zero, whereas the total strain is 8 strain units ($= 800\%$). At the lab-frame strain extreme, therefore, the structure experiences little-to-no deformation and hence exhibits no recoverable strain. This is also confirmed by regaining quiescent scattering characteristics at $\gamma_{\text{rec}} = 0$ in Figs. 8 and 9. This finding, that the structure is restored to its equilibrium configuration at the (total) strain extremes agrees with a number of recent experimental and simulational studies of polymeric and colloidal systems under LAOS [15,19–27, 55], where a constant linear-regime elasticity exists near the strain extrema. Here, we exploit *in situ* SANS to structurally confirm these bulk-rheological observations in a much softer system than has been previously investigated and conclude these observations can be well understood from the viewpoint of recoverable (material-frame) strain.

In the right panel in Fig. 10, we show that the recoverable strain is closely correlated to the alignment factor.

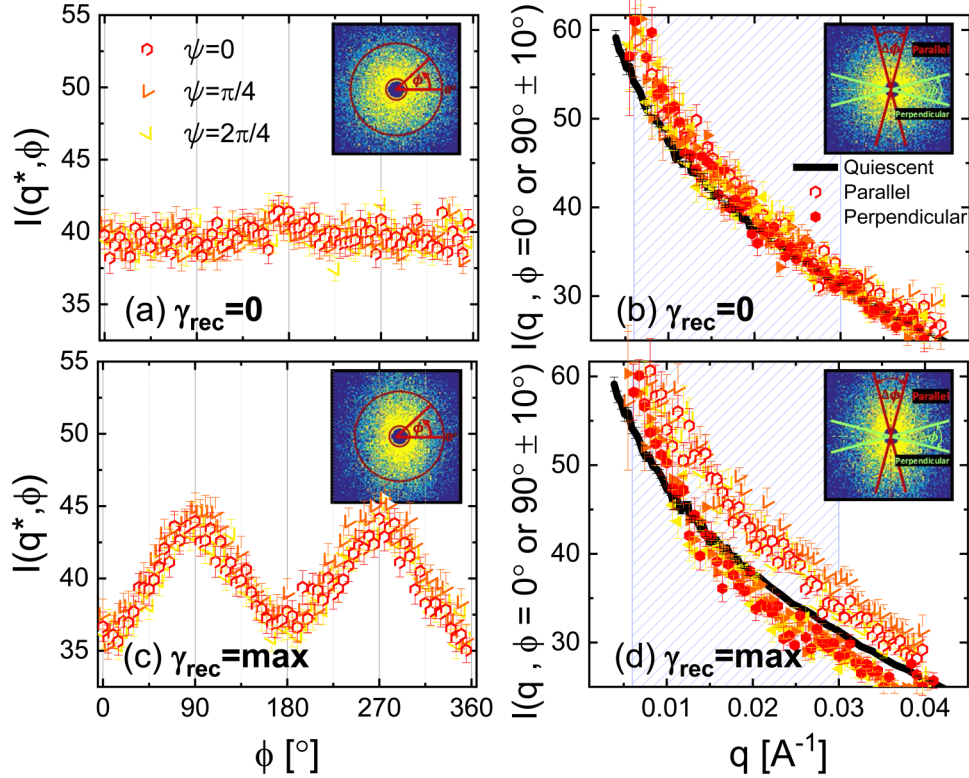


FIG. 9. Rheo-SANS performed at the instants of $\gamma_{\text{rec}} = 0$ [(a) and (b)] and $\gamma_{\text{rec}} = \text{max}$ [(c) and (d)], displayed as 1D annular-averaged SANS intensity $I(q^*, \phi)$ [(a) and (c)] and 1D sector-averaged SANS parallel ($\phi = 90^\circ \pm 10^\circ$) and perpendicular ($\phi = 0^\circ \pm 10^\circ$) to the orientation angle [(b) and (d)]. The stress input with different stress phases $\psi = 0, \pi/4$, and $2\pi/4$ results in the indistinguishable SANS. Sample 2D patterns are shown in the inset.

The alignment factor has no directional dependence and, therefore, is always positive. We see a remarkable structure-property relationship: when the recoverable strain magnitude $|\gamma_{\text{rec}}|$ is small, the Kuhn segments are isotropically arranged. As the magnitude of the recoverable strain increases due to imposed deformations, more of the Kuhn segments are aligned in the flow direction.

While there is a distinct shifting observed in the (total) strain, we see that the recoverable strain contains no shifting and always oscillates about zero, resulting in properties that match with the microstructure. We, therefore, establish a structure-property-processing relationship, $A_f \propto |\gamma_{\text{rec}}|$. We, therefore, see that distinct information is encoded in the total and recoverable strains. The (total) strain shift contains information relating to the shear viscosity as demonstrated, whereas the recoverable strain reveals the amount of microscopic deformation that structure experiences, as supported by our SANS measurements.

F. Application to stiffer materials

In this section, we demonstrate ways in which the information provided from the strain shifts can be useful in studying gels and polymer melts. In linear viscoelasticity, the strain shift is directly related to the zero-shear viscosity as shown earlier in Sec. III D. Rearranging Eq. (15) gives the expression for zero-shear viscosity,

$$\eta_0 = \frac{\sigma_0}{\omega \gamma_S} \cos \psi. \quad (18)$$

Equation (18) provides an alternative, fast way to determine the zero-shear viscosity for viscoelastic materials. In addition, we can use it to establish an approach by which a stress (torque)-controlled instrument can be used to obtain equivalent information that typically is only available from strain- or rate-controlled protocols without resorting to feedback loops. We observe that the zero-shear viscosity determined from steady shearing is equivalent to that from the strain shift for all the investigated materials.

A rapid determination of the zero-shear viscosity for materials that tend to experience edge fracture under steady shearing is appealing. As the protocol perturbs a material with minimal stress in an oscillatory manner, it prevents edge fracture and other experimental complexities associated with unidirectional shearing. We demonstrate the technique with numerous materials that are both viscous and notorious for edge fracture, including biological gels and polymer melts. The viscosities of these materials are normally difficult to be measured directly, and we show that the information can be precisely and efficiently acquired from the strain shifts.

1. Biological gels

We investigate three different biological systems that undergo a solgel transition [56], including collagen, PI-HA, and alginate. These natural biomaterials are widely used in applications such as drug-release [57], bioprinting [58], and bioencapsulation [59]. The states prior to and after the solgel transition are studied for each of the three

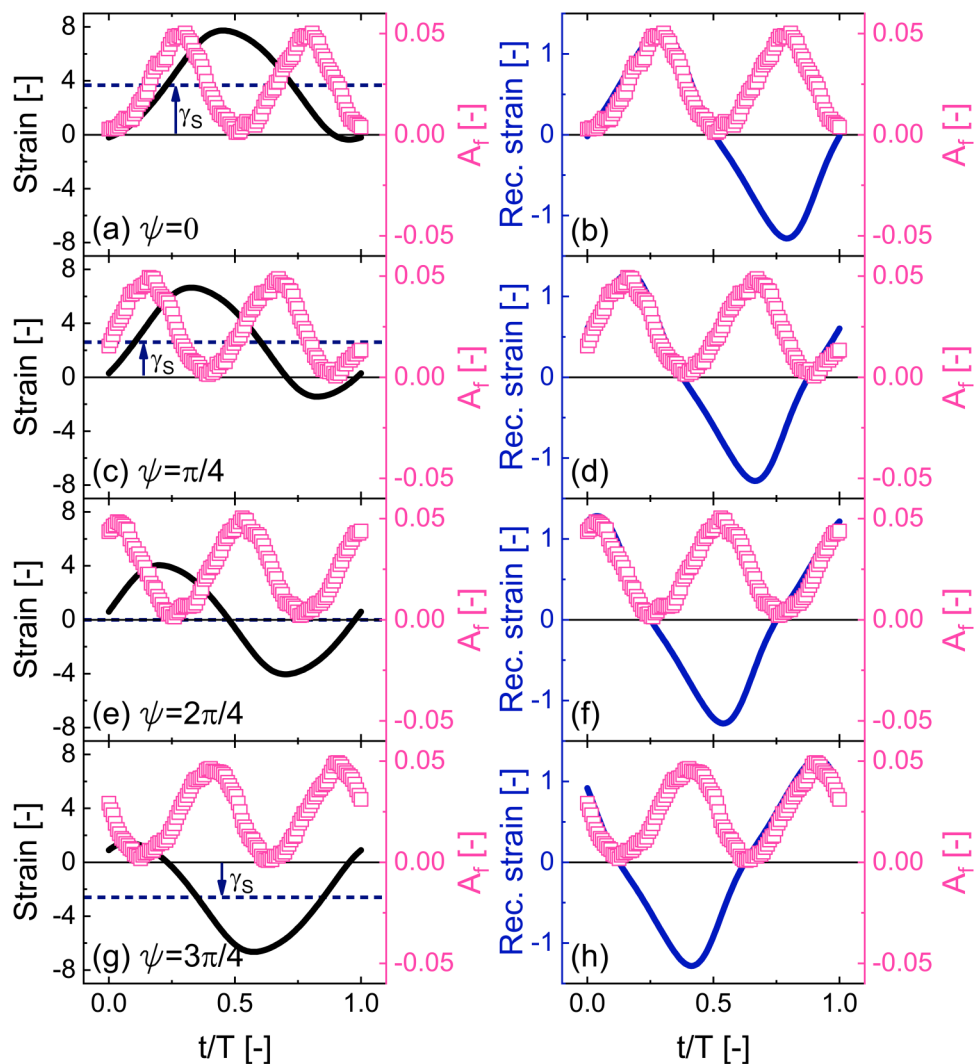


FIG. 10. Rheo-SANS study of PLMs. Total (lab-frame) strain γ [(a), (c), (e), and (g)] and recoverable (material-frame) strain γ_{rec} [(b), (d), (f), and (h)] are plotted on top of the temporal alignment factor (A_r). The data are taken under stress-controlled oscillatory shearing $\sigma(t) = \sigma_0 \sin(\omega t + \psi)$ with different stress phases $\psi=0$ [(a) and (b)], $\psi = \pi/4$ [(c) and (d)], $\psi = 2\pi/4$ [(e) and (f)], and $\psi = 3\pi/4$ [(g) and (h)]. The normalized time t/T is defined with respect to the impose stress $\sigma(t) = \sigma_0 \sin(\omega T(t/T) + \psi)$.

materials. The sol-state is essentially a polymer solution before any gelation events occur and is predominantly viscous, while the gel-state is when the material has eventually reached steady state after gelation has proceeded to completion.

The frequency dependence of the dynamic moduli $G'(\omega)$ and $G''(\omega)$ from the three materials are presented in Fig. 11. Before the gelation occurs, the sol-state shows G'' larger than G' across the frequency range, indicating the predominantly viscous nature. After the gelation process has completed, we observe little frequency dependence for the three systems, and the storage modulus is much larger than the loss modulus. These results collectively confirm that the materials have transitioned from the energy-dissipation-dominant sol-state into the energy-storage-dominant gel-state.

Once the materials fully transition into their gelled states, measurements such as steady shearing are experimentally not feasible, and SAOS measurements such as those presented in Fig. 11 are typically performed and used to interpret the

rheological properties of gels [60]. Other methods, such as taking the limit of $G''(\omega)/\omega$ as the frequency approaches zero cannot be accessed due to the significantly long relaxation processes that characterize many soft materials with high volume fractions. The shear viscosity is, therefore, not directly accessible. To this end, we demonstrate that the zero-shear viscosity can be easily obtained with a series of stress-controlled SAOS tests. Further, these biological gels are arguably more relevant to stress-driven protocols [61–64], as their applications such as ambulatory joint motion [65], and bioprinting [58] often involve stressing and force-loading processes.

We submit both the sol and gel states of each material to stress-controlled SAOS. The phase of the imposed stress is varied from $\psi = 0$ (sinusoidal stressing) to $\psi = \pi/2$ (cosinusoidal stressing). The corresponding normalized strain responses γ/γ_0 are presented in Fig. 12, where the sol and gel states are displayed on the left and right panels, respectively, for the three distinct systems. The strains from the sol-states clearly shift away from the origin with $\psi = 0$ and

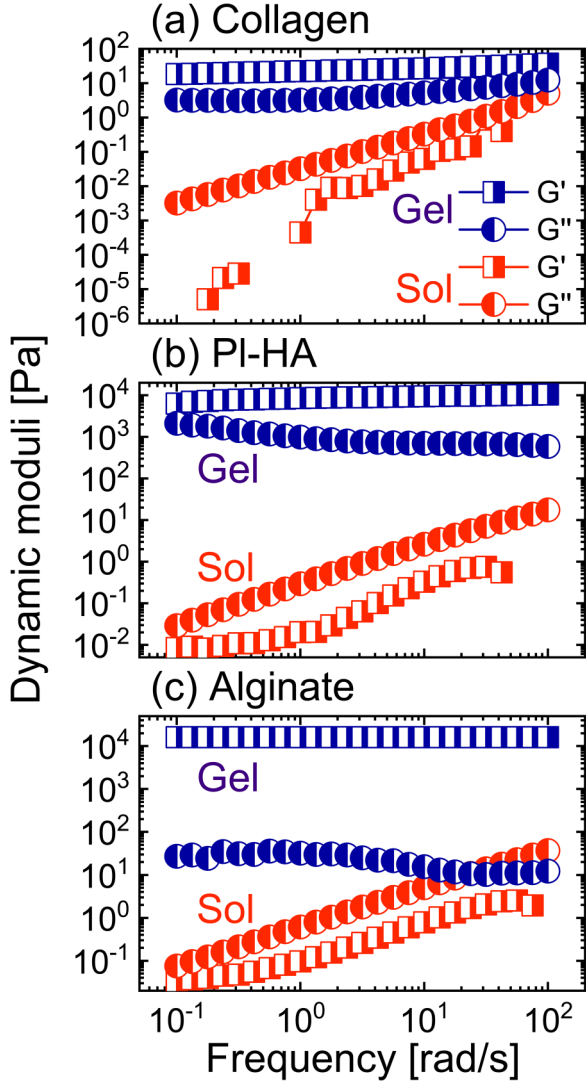


FIG. 11. Frequency dependence of the dynamic moduli $G'(\omega)$ and $G''(\omega)$ from the sol-state and gel-state of collagen (a), PI-HA (b), and alginate (c).

$\psi = \pi/4$, whereas $\psi = \pi/2$ gives rise to strain responses that oscillate about zero. The strain shifts are indicated with dashed lines. This again agrees with the previous results of PLMs and PEO solutions, and the prediction in Eq. (15) that strain responses to cosinusoidal stressing ($\psi = \pi/2$) contain no shifts.

In contrast to the viscous responses exhibited by the sol-states, the normalized strains of the gel states all essentially oscillate about zero strain, with the three different phases. The very small shifts we do measure, with their associated experimental uncertainties, indicate that the viscosities are so high that the materials can be treated as solids.

The strain shifts are presented in Table I, normalized by the stress amplitude, γ_S/σ_0 . This normalized shift is independent of the stress amplitude in the linear viscoelastic regime and is equal to $\cos\psi/\omega\eta_0$, according to Eq. (15). This material-dependent parameter γ_S/σ_0 is displayed in Table I from the stress phases of 0 and $\pi/4$, while the shifts are zero in the case of cosinusoidal stressing ($\psi = \pi/2$).

Following Eq. (18), the zero-shear viscosities are calculated and presented in Table I. In the sol-state where the shifts are significant, the viscosities are constant for each system regardless of ψ and are determined to be about 0.035, 0.29, and 0.71 Pa·s for the collagen, PI-HA, and alginate, respectively. Once the materials have gelled, the viscosity is increased significantly by the cross-linking of the network. The zero-shear viscosities of the gel-state are tabulated in Table I, which increase 3, 5, and 7 orders of magnitude from the sol-state for collagen, PI-HA, and alginate, respectively. The difference in viscosity in the collagen and PI-HA gels is due to the physical cross-links, while the alginate gel is by covalent cross-links. In this case, the strain shifts from the origin are as small as 10^{-5} strain units, resulting in large uncertainties that are dictated by the measurement capability of the rheometer used. Despite such uncertainties, we observe roughly constant zero-shear viscosities at the two stress phases (ψ) for each gel.

In addition to the already wide adoption of SAOS, this technique provides a novel way for directly determining the zero-shear viscosity of biological gels.

2. Polymer melts

The success and efficiency of processing molten polymers is often highly dependent on their flow properties. From a molecular perspective, the zero-shear viscosity provides important information regarding their size and architecture. Nevertheless, zero-shear viscosity data are not always directly accessible, as edge fracture often complicates the collection of clean steady-shear data.

Alternatively, researchers often perform a series of SAOS tests at various temperatures, and then use the TTS principle [4] to superimpose the dynamic moduli to construct a master curve that accommodates the widest possible range of time scales. With the master curve determined, the zero-shear viscosity is typically determined by taking the limit of G''/ω as the frequency approaches zero,

$$\eta_0 = \lim_{\omega \rightarrow 0} G''/\omega. \quad (19)$$

This relation relies on being able to access the terminal relaxation regime.

The process of superposition relies on the determination of shift factors, including the horizontal a_T and vertical b_T shift factors. The shift factors relate the value of a property measured at a temperature T to that of the reference temperature T_{ref} [66]. A material property such as the zero-shear viscosity at a temperature T can, therefore, be linked to the reference temperature T_{ref} by

$$\eta_0(T) = \frac{a_T(T)}{b_T(T)} \eta_0(T_{\text{ref}}). \quad (20)$$

The vertical shift factor, which relates the density of the polymer at a temperature T to the density at the reference temperature, T_{ref} , is usually close to unity $b_T \approx 1$ for moderate temperature differences in homopolymers. The horizontal

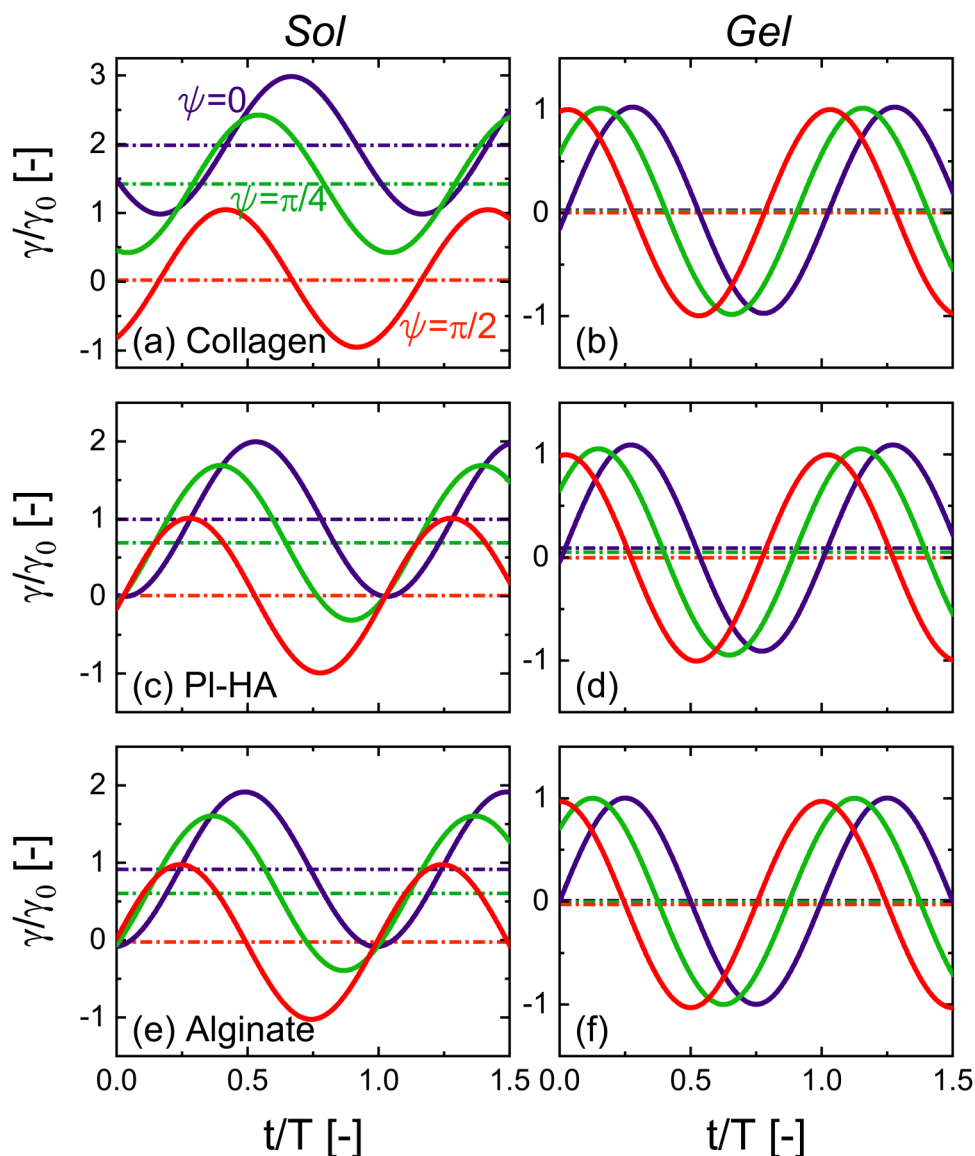


FIG. 12. Strain response from collagen [(a) and (b)], PI-HA [(c) and (d)], and alginate [(e) and (f)] in the corresponding sol- and gel-phase at an angular frequency of 0.5 rad/s. The stress is imposed with varying phases of ψ of 0 (blue), $\pi/4$ (green), and $\pi/2$ (red), and the corresponding strain shifts are labeled as dashed lines.

shift factor can, therefore, be determined from the zero-shear viscosity as

$$a_T(T) = \frac{\eta_0(T)}{\eta_0(T_{ref})}. \quad (21)$$

The relationship in Eq. (21), which is also theoretically predicted in molecular models such as those attributed to Rouse [67] and Doi and Edwards [32], offers a direct way to determine the horizontal shift factors based on material properties, rather than relying on specific postprocessing algorithms that minimize the difference between the shifted curves [68,69]. Despite being theoretically robust, Eq. (21) is not commonly used to quantify the shift factors because of experimental difficulties in measuring the zero-shear viscosity. Conventionally, the information regarding zero-shear viscosity is extracted from an already superimposed master curve, which restricts the application of Eq. (21).

We investigate two molten PS samples with molecular weights of 14 000 (PS-14k) and 46 000 (PS-46k). We show that the TTS shift factors, determined by exploiting the link between the strain shifts and zero-shear viscosities, can be obtained as in Eq. (21) without the use of a fitting algorithm. The master curve of PS-46k is displayed in Fig. 13(a) as $G'(a_T\omega)$ and $G''(a_T\omega)$, with the colors coded for different measurement temperatures. The G''/ω is presented on the right y axes, where the zero-shear viscosity is quantified to be $\eta_0 \approx 1.7 \times 10^4$ Pa s following Eq. (19). A van Gurp–Palmen-plot (vGP-plot) is shown in Fig. 13(b) to confirm the superposition quality [70] as the data collected from individual temperatures form a continuous curve without vertical shifting ($b_T = 1$). The local minimum in the vGP-plot is interpreted as indicating that the sample is entangled ($M_e \approx 135\,000$) [71] and that the plateau modulus is $G_N^0 \approx 2 \times 10^5$ Pa, in agreement with previous studies of PS [72].

TABLE I. Strain shifts and zero-shear viscosities determined from the three distinct biological systems in corresponding sol- and gel-phase.

Material	ψ	Sol-state		Gel-state	
		γ_S/σ_0 (1/Pa)	η_0 (Pa s)	γ_S/σ_0 (1/Pa)	η_0 (Pa s)
Collagen	0	57.53	0.0348 ± 0.001	4.71×10^{-3}	424.63 ± 26
	$\pi/4$	41.27	0.0343 ± 0.001	2.98×10^{-3}	474.56 ± 32
PI-HA	0	6.87	0.291 ± 0.004	1.09×10^{-5}	$1.84 \times 10^5 \pm 0.42 \times 10^5$
	$\pi/4$	4.77	0.297 ± 0.007	6.44×10^{-6}	$2.18 \times 10^5 \pm 0.63 \times 10^5$
Alginate	0	2.80	0.714 ± 0.08	1.27×10^{-7}	$1.57 \times 10^7 \pm 2.1 \times 10^7$
	$\pi/4$	1.31	0.763 ± 0.1	5.94×10^{-8}	$2.64 \times 10^7 \pm 3.52 \times 10^7$

The TTS horizontal shift factors a_T that are used to construct the master curve are presented as a function of measurement temperature in Fig. 14. The WLF model is used to fit the data and is shown as a dashed line. The WLF fit parameters in Eq. (9) are $C_1 = 6.15$ and $C_2 = 98.48$ K. We further perform a series of stress-controlled SAOS measurements across the same temperature range, extracting the strain shifts γ_S . Following Eq. (18), the zero-shear viscosity at each temperature is subsequently determined. The horizontal shift factors are then calculated as indicated in Eq. (21) and presented in Fig. 14 as red stars. We observe that the TTS shift factors determined from the strain shift are consistent with the WLF model fit determined by the algorithm employed by TRIOS. The strain shifts below 130°C are smaller than 10^{-5} and experimentally unresolvable due to rheometer

measurement limitation, as the polymer melt approaches its glassy regime. The results from PS-14k are included in Appendix, and the same equivalence of TTS shift factors is obtained.

Finally, the zero-shear viscosity determined from the strain shift is displayed in Fig. 15 (right axis), where the viscosity determined at each temperature is related to the reference temperature by presenting $\eta_0(T)/a_T(T)$. While the zero-shear viscosity is typically taken from data in the terminal regime, we observe that the zero-shear viscosity can be determined well above the terminal regime, by over one decade in frequency. The highest frequency at which a constant η_0 is determined corresponds to the frequency at which the plateau modulus G_N^0 is observed. It is expected that η_0 would not stay constant and ought to decrease with further increases in frequency. Further investigation of the frequency dependence using the strain shift effect is restricted by the current capability of a rheometer and is outside the scope of this work.

Overall, we have demonstrated that the strain shift can be used to efficiently determine the zero-shear viscosity of polymer melts and that the approach can be further applied to determine the TTS shift factors in an algorithm-free manner.

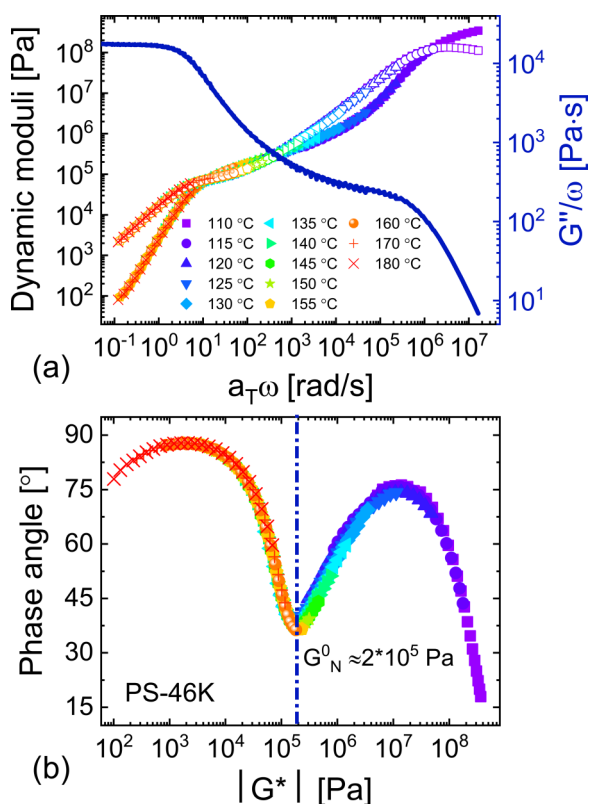


FIG. 13. Master curve of PS-46k constructed at a reference temperature of 155°C (a) and the vGP-plot (b); the dashed line in the vGP-plot indicates the minimum of phase angle, where the plateau modulus $G_N^0 \approx 2 \times 10^5$ Pa is defined.

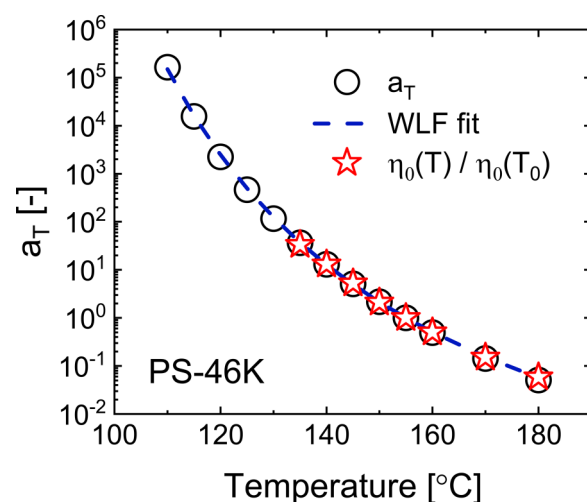


FIG. 14. Horizontal shift factors of TTS from PSk-46k at $T_{\text{ref}} = 155^\circ\text{C}$. The dashed line represents the fitting from the WLF equation ($C_1 = 6.15$ and $C_2 = 98.48$ K), and the red stars are determined from strain shifts following Eqs. (18) and (21).

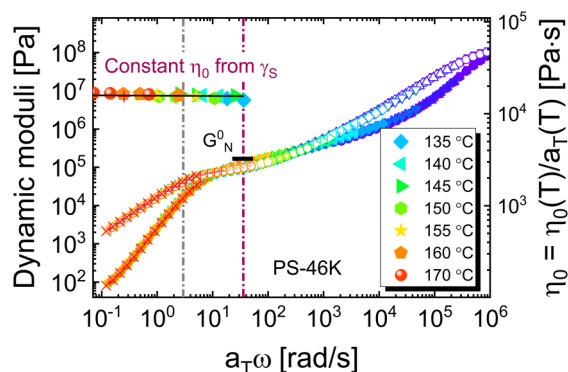


FIG. 15. The zero-shear viscosity η_0 (determined from strain shifts) as the function of shifted frequency ($a_T\omega$). The gray dashed line represents the terminal regime where a constant G''/ω is observed; the (dark red) dashed line indicates the extensive regime where the constant zero-shear viscosity is shown from the strain-shift approach. The boundary of the observed constant zero-shear viscosity corresponds to the frequency where the plateau modulus G_N^0 is typically defined.

IV. CONCLUSION AND OUTLOOK

The phenomenology of strain responses being shifted from the origin under stress-driven oscillatory shearing has been extensively investigated. We have presented a simple theory of strain shifting under oscillatory stressing that follows the same approach as that used to determine the unrecoverable strain in traditional creep and recovery tests. Our theory is based on the concepts of recovery rheology [15,18,42,43], where the strain shift depends on the zero-shear viscosity and three experimental parameters including the stress amplitude, the imposed frequency, and *the phase of the imposed stress*. The theoretical prediction is experimentally validated with measurements from two polymeric systems including entangled PLMs and PEO solutions. An approach to probing the zero-shear viscosity has, therefore, been established, and it is shown that this approach agrees with the steady-shearing results and could be more efficient and practical for a range of complex materials.

Rheo-SANS is used to show that the strain shifting phenomenon does not affect the microstructure. While distinct strain shifts are observed for the total strain, the recoverable strain contains no shifting and always oscillates about the origin. The recoverable strain is also observed to correlate to segmental alignment regardless of flow conditions, resulting in a distinct structure-property-processing relationship, $A_F \propto |\gamma_{rec}|$. We, therefore, conclude that the recoverable strain reveals the microscopic deformation [15] and the total strain shift contains information relating to the shear viscosity.

The approach is further applied to a wide variety of materials, including biological gels and polymer melts that fracture at the edges when subjected to large strains and strain rates. While steady shearing for long times is typically not feasible for these stiff materials, measuring the strain shift allows us to determine their zero-shear viscosities efficiently and accurately. In particular, for polymer melts, with this rapid determination of zero-shear viscosity, we have shown that the horizontal shift factors of TTS can be experimentally determined in an algorithm-free manner and are consistent with the WLF model.

Past work has raised the question of whether it is better to use sinusoidal or cosinusoidal stresses for oscillatory stress

rheometry. Cosinusoidal stresses have been suggested because of the convenience of retaining positivity in Fourier harmonics in nonlinear tests. We conclusively address this question in this work, by showing and explaining the physicality of both approaches, as well as every other phase shift one may wish to implement. In short, one can clearly obtain viscosity information, free from any elastic effects, from sinusoidal stressing, while cosinusoidal stressing will force the total strains to oscillate about zero. While cosinusoidal stressing conveniently leads to the strain oscillating about the starting point of the experiment, it does so at the expense of being able to easily determine the zero-shear viscosity. Both approaches, therefore, have their respective merits.

The results of this study, when viewed in the context of our recent work [15], indicate the emergence of a more nuanced view of experimental determinations of viscoelastic responses from oscillatory shearing. We have shown that the recoverable strain and unrecoverable strain rate are the primary measurables that relate to the determination of moduli and viscosities. The recoverable strain dictates the elasticity by creating a more ordered and more aligned configuration that is entropically unfavorable, and the rate at which strain is acquired unrecoverably determines the flow viscosity. These metrics that define elastic and viscous responses, the recoverable strain and unrecoverable strain rate, are not necessarily in-phase with the total strain or the total strain rate. This view may seem at odds with the typical assumption applied to linear-regime oscillatory rheology that elastic behaviors are in-phase with the (total) strain, while viscous behaviors are in-phase with the (total) strain rate. It is not. The dynamic moduli, G' and G'' , which are the prefactors of the in- and out-of-phase components of the oscillatory output, are proportional to the average energy stored per unit volume of the material over a cycle of the excitation and the energy dissipated per unit volume of the material over a cycle of deformation [5]. To accurately determine the *instantaneous* energetic terms, which then get averaged to calculate the dynamic moduli, one must know the elastic deformation and the rate at which deformation is acquired viscously. These can be measured via recovery tests [15], or by measuring the strain shift under oscillatory stressing, as we have shown here.

In summary, we provide a theoretical, bulk-rheological, and structural understanding of strain shifting under oscillatory stresses. The information that is unveiled in the work can be generally applied to any viscoelastic materials, which paves a rigorous and efficient approach to measure the zero-shear viscosity.

ACKNOWLEDGMENTS

The authors thank Professor Dimitris Vlassopoulos for invaluable comments on an early version of the manuscript. Discussions with Dr. David Bohnsack and Dr. Bharath Rajaram from TA Instruments and Dr. Abhi Shetty from Anton Paar are gratefully acknowledged. The authors thank Dylan Walsh and Professor Damien Guirionnet for providing polystyrene samples. Access to NBG 30m-SANS was provided by the Center for High Resolution Neutron Scattering, a partnership between the National Institute of Standards and Technology

(NIST) and the National Science Foundation (NSF) under Agreement No. DMR-1508249. This material is based upon work supported by the National Science Foundation (NSF) under Grant No. 1727605. Certain commercial instruments or materials are identified in this paper to foster understanding. Such identification does not imply recommendation or endorsement by the National Institute of Standards and Technology nor does it imply that the materials or equipment identified are necessarily the best available for the purpose. H.K. acknowledges the funding provided by the National Science Foundation STC-EBICS Grant CBET-0939511

Postscript: We have recently been made aware of the development of a theory based on the results presented here. While our work deals exclusively with the steady state alternating case, this new work, which confirms our major findings, considers the initial transience from startup.

APPENDIX: ADDITIONAL DATA FROM PS-14K

Figure 16 contains the data from PS-14K. The master curve is first presented in Fig. 16(a), followed by the

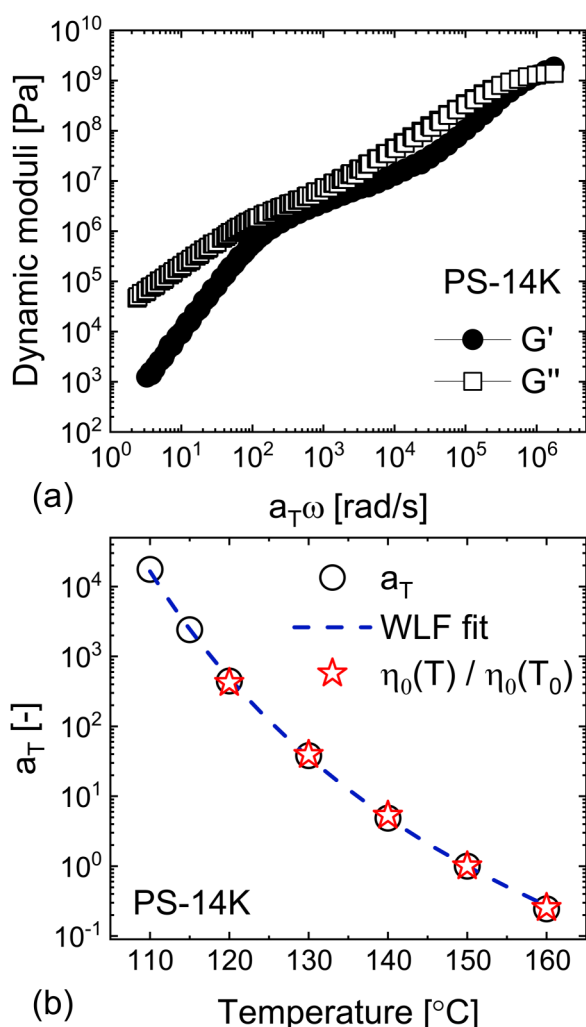


FIG. 16. (a) Master curve of polystyrene-14K constructed at a reference temperature of 150 $^{\circ}$ C. (b) Horizontal shift factors of TTS from PS-14K. The dashed line represents the fitting from WLF equation ($C_1 = 5.99$ and $C_2 = 97.80$ K), and the red stars are the TTS shifting factors determined from strain shifts from Eq. (21).

horizontal shift factors collected at numerous temperatures in Fig. 16(b). Similar to PS-46K, the determination of horizontal shift factors from Eq. (21) using strain shifts agrees with the WLM model fit.

REFERENCES

- [1] Hyun, K., M. Wilhelm, C. O. Klein, K. S. Cho, J. G. Nam, K. H. Ahn, S. J. Lee, R. H. Ewoldt, and G. H. McKinley, "A review of nonlinear oscillatory shear tests: Analysis and application of large amplitude oscillatory shear (LAOS)," *Prog. Polym. Sci.* **36**, 1697–1753 (2011).
- [2] Rogers, S., "Large amplitude oscillatory shear: Simple to describe, hard to interpret," *Phys. Today* **71**, 34–40 (2018).
- [3] Jaspers, M., S. L. Vaessen, P. van Schayik, D. Voerman, A. E. Rowan, and P. H. J. Kouwer, "Nonlinear mechanics of hybrid polymer networks that mimic the complex mechanical environment of cells," *Nat. Commun.* **8**, 15478 (2017).
- [4] Ferry, J. D., *Viscoelastic Properties of Polymers* (Wiley, New York, 1980).
- [5] Tschoegl, N. W., *The Phenomenological Theory of Linear Viscoelastic Behavior* (Springer, Berlin, 1989).
- [6] Ad Hoc Committee on Official Nomenclature and Symbols, "Official symbols and nomenclature of The Society of Rheology," *J. Rheol.* **57**, 1047–1055 (2013).
- [7] Hyun, K., S. H. Kim, K. H. Ahn, and S. J. Lee, "Large amplitude oscillatory shear as a way to classify the complex fluids," *J. Nonnewton. Fluid Mech.* **107**, 51–65 (2002).
- [8] Lauger, J., K. Wollny, and S. Huck, "Direct strain oscillation: A new oscillatory method enabling measurements at very small shear stresses and strains," *Rheol. Acta* **41**, 356–361 (2002).
- [9] Bae, J. E., M. Lee, K. S. Cho, K. H. Seo, and D. G. Kang, "Comparison of stress-controlled and strain-controlled rheometers for large amplitude oscillatory shear," *Rheol. Acta* **52**, 841–857 (2013).
- [10] Lauger, J., and H. Stettin, "Differences between stress and strain control in the non-linear behavior of complex fluids," *Rheol. Acta* **49**, 909–930 (2010).
- [11] Dimitriou, C. J., R. H. Ewoldt, and G. H. McKinley, "Describing and prescribing the constitutive response of yield stress fluids using large amplitude oscillatory shear stress (LAOSTress)," *J. Rheol.* **57**, 27–70 (2013).
- [12] de Souza Mendes, P. R., R. L. Thompson, A. A. Alicke, and R. T. Leite, "The quasilinear large-amplitude viscoelastic regime and its significance in the rheological characterization of soft matter," *J. Rheol.* **58**, 537–561 (2014).
- [13] Ewoldt, R. H., "Defining nonlinear rheological material functions for oscillatory shear," *J. Rheol.* **57**, 177–195 (2013).
- [14] Shan, L., H. He, N. J. Wagner, and Z. Li, "Nonlinear rheological behavior of bitumen under LAOS stress," *J. Rheol.* **62**, 975–989 (2018).
- [15] Lee, J. C.-W., K. M. Weigandt, E. G. Kelley, and S. A. Rogers, "Structure-property relationships via recovery rheology in viscoelastic materials," *Phys. Rev. Lett.* **122**, 248003 (2019).
- [16] Munster, S., L. M. Jawerth, B. A. Leslie, J. I. Weitz, B. Fabry, and D. A. Weitz, "Strain history dependence of the nonlinear stress response of fibrin and collagen networks," *Proc. Natl. Acad. Sci. U.S.A.* **110**, 12197–12202 (2013).
- [17] Pipkin, A. C., *Lectures on Viscoelasticity Theory*, Applied Mathematical Sciences Vol. 7 (Springer, New York, NY, 1986).
- [18] Lee, J. C.-W., L. Porcar, and S. Rogers, "Recovery rheology via rheo-SANS: Application to step strains under out-of-equilibrium conditions," *AICHE J.* (2019).

- [19] Rogers, S. A., B. M. Erwin, D. Vlassopoulos, and M. Cloitre, "A sequence of physical processes determined and quantified in LAOS: Application to a yield stress fluid," *J. Rheol.* **55**, 435–458 (2011).
- [20] Kim, J., D. Merger, M. Wilhelm, and M. E. Helgeson, "Microstructure and nonlinear signatures of yielding in a heterogeneous colloidal gel under large amplitude oscillatory shear," *J. Rheol.* **58**, 1359–1390 (2014).
- [21] Lee, C.-W., and S. A. Rogers, "A sequence of physical processes quantified in LAOS by continuous local measures," *Korea-Aust. Rheol. J.* **29**, 269–279 (2017).
- [22] Rogers, S. A., "In search of physical meaning: Defining transient parameters for nonlinear viscoelasticity," *Rheol. Acta* **56**, 501–525 (2017).
- [23] Ramya, K. A., J. Kodavaty, P. Dorishetty, M. Setti, and A. P. Deshpande, "Characterizing the yielding processes in pluronic-hyaluronic acid thermoreversible gelling systems using oscillatory rheology," *J. Rheol.* **63**, 215–228 (2019).
- [24] Park, J. D., and S. A. Rogers, "The transient behavior of soft glassy materials far from equilibrium," *J. Rheol.* **62**, 869–888 (2018).
- [25] Radhakrishnan, R., and S. M. Fielding, "Shear banding of soft glassy materials in large amplitude oscillatory shear," *Phys. Rev. Lett.* **117**, 188001 (2016).
- [26] Deshpande, A. P., *Oscillatory Shear Rheology for Probing Nonlinear Viscoelasticity of Complex Fluids: Large Amplitude Oscillatory Shear* (Springer, New York, 2010).
- [27] van der Vaart, K., Y. Rahmani, R. Zargar, Z. Hu, D. Bonn, and P. Schall, "Rheology of concentrated soft and hard-sphere suspensions," *J. Rheol.* **57**, 1195–1209 (2013).
- [28] Lee, J. C.-W., L. Porcar, and S. A. Rogers, "Unveiling temporal nonlinear structure–rheology relationships under dynamic shearing," *Polymers* **11**, 1189 (2019).
- [29] Ravindranath, S., and S.-Q. Wang, "Universal scaling characteristics of stress overshoot in startup shear of entangled polymer solutions," *J. Rheol.* **52**, 681–695 (2008).
- [30] Wang, Y., X. Li, X. Zhu, and S. Q. Wang, "Characterizing state of chain entanglement in entangled polymer solutions during and after large shear deformation," *Macromolecules* **45**, 2514–2521 (2012).
- [31] Wang, S. Q., Y. Wang, S. Cheng, X. Li, X. Zhu, and H. Sun, "New experiments for improved theoretical description of nonlinear rheology of entangled polymers," *Macromolecules* **46**, 3147–3159 (2013).
- [32] Doi, M., and S. Edwards, *The Theory of Polymer Dynamics* (Oxford University, Oxford, 1986).
- [33] Lin, Y. H., "Comparison of experiment and the proposed general linear viscoelastic theory. 2. Stress relaxation line shape analysis," *Macromolecules* **19**, 159–168 (1986).
- [34] Klein, J., "The onset of entangled behavior in semidilute and concentrated polymer solutions," *Macromolecules* **11**, 852–858 (1978).
- [35] Dalsin, S. J., M. A. Hillmyer, and F. S. Bates, "Molecular weight dependence of zero-shear viscosity in atactic polypropylene bottlebrush polymers," *ACS Macro Lett.* **3**, 423–427 (2014).
- [36] Giacomin, A. J., R. B. Bird, L. M. Johnson, and A. W. Mix, "Large-amplitude oscillatory shear flow from the corotational Maxwell model," *J. Nonnewton. Fluid Mech.* **166**, 1081–1099 (2011).
- [37] Schweizer, T., J. van Meerveld, and H. C. Öttinger, "Nonlinear shear rheology of polystyrene melt with narrow molecular weight distribution—Experiment and theory," *J. Rheol.* **48**, 1345–1363 (2004).
- [38] Meissner, J., R. W. Garbella, and J. Hostettler, "Measuring normal stress differences in polymer melt shear flow," *J. Rheol.* **33**, 843–864 (2002).
- [39] Sniijkers, F., and D. Vlassopoulos, "Cone-partitioned-plate geometry for the ARES rheometer with temperature control," *J. Rheol.* **55**, 1167–1186 (2011).
- [40] Cox, W. P., and E. H. Merz, "Correlation of dynamic and steady flow viscosities," *J. Polym. Sci. A* **28**, 619–622 (1958).
- [41] Worsfold, D. J., and S. Bywater, "Anionic polymerization of styrene," *Can. J. Chem.* **38**, 1891–1900 (1960).
- [42] Weissenberg, K., "A continuum theory of rheological phenomena," *Nature* **159**, 310–311 (1947).
- [43] Lodge, A. S., "A network theory of constrained elastic recovery in concentrated polymer solutions," *Rheol. Acta* **1**, 158–163 (1958).
- [44] Eberle, A. P. R., and L. Porcar, "Flow-SANS and Rheo-SANS applied to soft matter," *Curr. Opin. Colloid Interface Sci.* **17**, 33–43 (2012).
- [45] Kline, S. R., "Reduction and analysis of SANS and USANS data using IGOR Pro," *J. Appl. Crystallogr.* **39**, 895–900 (2006).
- [46] Calabrese, M. A., N. J. Wagner, and S. A. Rogers, "An optimized protocol for the analysis of time-resolved elastic scattering experiments," *Soft Matter* **12**, 2301–2308 (2016).
- [47] Mooney, M., "Secondary stresses in viscoelastic flow," *J. Colloid Sci.* **6**, 96–107 (1951).
- [48] Benbow, J. J., and E. R. Howells, "Normal stress, shear recovery and viscosity in polydimethyl siloxanes," *Polymer* **2**, 429–436 (1961).
- [49] Wagner, M. H., and H. M. Laun, "Nonlinear shear creep and constrained elastic recovery of a LDPE melt," *Rheol. Acta* **17**, 138–148 (1978).
- [50] Laun, H. M., "Prediction of elastic strains of polymer melts in shear and elongation," *J. Rheol.* **30**, 459–501 (1986).
- [51] Reh binder, P., "Coagulation and thixotropic structures," *Discuss. Faraday Soc.* **18**, 151–160 (1954).
- [52] Muenstedt, H., N. Katsikis, and J. Kaschta, "Rheological properties of poly(methyl methacrylate)/nanoclay composites as investigated by creep recovery in shear," *Macromolecules* **41**, 9777–9783 (2008).
- [53] Rogers, S. A., J. D. Park, and C.-W. J. Lee, "Instantaneous dimensionless numbers for transient nonlinear rheology," *Rheol. Acta* **58**, 539–556 (2019).
- [54] Reiner, M., *Encyclopedia of Physics VI* (Springer, Berlin, 1958), pp. 435–549.
- [55] Lee, J. C.-W., J. D. Park, and S. A. Rogers, "Studying large amplitude oscillatory shear response of soft materials," *J. Vis. Exp.* **146**, e58707 (2019).
- [56] Winter, H. H., and F. Chambon, "Analysis of linear viscoelasticity of a crosslinking polymer at the gel point," *J. Rheol.* **30**, 367–382 (1986).
- [57] Friess, W., "Collagen—Biomaterial for drug delivery," *Eur. J. Pharm. Biopharm.* **45**, 113–136 (2002).
- [58] Murphy, S. V., A. Skardal, and A. Atala, "Evaluation of hydrogels for bio-printing applications," *J. Biomed. Mater. Res. A* **101A**, 272–284 (2013).
- [59] Avnir, D., O. Lev, and J. Livage, "Recent bio-applications of sol-gel materials," *J. Mater. Chem.* **16**, 1013–1030 (2006).
- [60] Sun Han Chang, R., J. C.-W. Lee, S. Pedron, B. A. C. Harley, and S. A. Rogers, "Rheological analysis of the gelation kinetics of an enzyme cross-linked PEG hydrogel," *Biomacromolecules* **20**, 2198–2206 (2019).
- [61] Chaudhuri, O., S. H. Parekh, and D. A. Fletcher, "Reversible stress softening of actin networks," *Nature* **445**, 295–298 (2007).
- [62] Broedersz, C. P., K. E. Kasza, L. M. Jawerth, S. Münster, D. A. Weitz, and F. C. MacKintosh, "Measurement of nonlinear rheology of cross-linked biopolymer gels," *Soft Matter* **6**, 4120–4127 (2010).
- [63] Licup, A. J., S. Münster, A. Sharma, M. Sheinman, L. M. Jawerth, B. Fabry, D. A. Weitz, and F. C. MacKintosh, "Stress controls the mechanics of collagen networks," *Proc. Natl. Acad. Sci. U.S.A.* **112**, 9573–9578 (2015).
- [64] Das, R. K., V. Gocheva, R. Hammink, O. F. Zouani, and A. E. Rowan, "Stress-stiffening-mediated stem-cell commitment switch in soft responsive hydrogels," *Nat. Mater.* **15**, 318–325 (2016).

- [65] Zhang, Z., and G. F. Christopher, "The nonlinear viscoelasticity of hyaluronic acid and its role in joint lubrication," *Soft Matter* **11**, 2596–2603 (2015).
- [66] Dealy, J., and D. Plazek, "Time-temperature superposition—A users guide," *Rheol. Bull.* **78**, 16–31 (2009).
- [67] Rouse, P. E., "A theory of the linear viscoelastic properties of dilute solutions of coiling polymers," *J. Chem. Phys.* **21**, 1272–1280 (1953).
- [68] Bae, J. E., K. S. Cho, K. H. Seo, and D. G. Kang, "Application of geometric algorithm of time-temperature superposition to linear viscoelasticity of rubber compounds," *Korea-Aust. Rheol. J.* **23**, 81–87 (2011).
- [69] Naya, S., A. Meneses, J. Tarrío-Saavedra, R. Artiaga, J. López-Beceiro, and C. Gracia-Fernández, "New method for estimating shift factors in time-temperature superposition models," *J. Therm. Anal. Calorim.* **113**, 453–460 (2013).
- [70] Van Gurp, M., and J. Palmen, "Time-temperature superposition for polymeric blends," *Rheol. Bull.* **67**, 5–8 (1998).
- [71] Lin, Y.-H., "Entanglement and the molecular weight dependence of polymer glass transition temperature," *Macromolecules* **23**, 5292–5294 (1990).
- [72] Liu, C. Y., J. S. He, E. van Ruymbeke, R. Keunings, and C. Bailly, "Evaluation of different methods for the determination of the plateau modulus and the entanglement molecular weight," *Polymer* **47**, 4461–4479 (2006).
- [73] See supplementary material at <https://doi.org/10.1122/1.5111358> for the frequency dependence of the PLMs and PEO solutions, the synthesis and characterization of polystyrene, and additional rheo-SANS data.